Continuum theory of negative surface energy: Resolving the paradox in quantum dots and nanostructures

Pradeep Sharma [*]

Program of Materials Science and Engineering, University of Houston, Houston, Texas 77204, USA; Department of Mechanical and Aerospace Engineering, University of Houston, Houston, Texas 77204, USA; and Department of Physics, University of Houston, Houston, Texas 77204, USA

(Received 25 June 2026; accepted 17 August 2026; published 11 September 2026)

Calvin *et al.* [Proc. Natl. Acad. Sci. USA **121**, e2307633121 (2024)] recently reported a result that sounds thermodynamically forbidden: semiconductor quantum dots with negative surface energy. If creating surface area lowers a system's free energy, why do these materials not spontaneously subdivide into oblivion? As Calvin *et al.* qualitatively recognized, this paradox vanishes because a ligand-capped nanocrystal is not a pristine solid-vacuum boundary, but a chemically open system where favorable ligand adsorption can drive the scalar surface excess negative. In this work, we formalize this physical distinction by extending the theory of continuum surface mechanics to account for chemically open, ligand-decorated surfaces. Our framework decouples the scalar calorimetric excess from its mechanical derivatives, illustrating that an apparent negative surface energy implies neither negative surface stress nor mechanical instability. Furthermore, this open-system formulation predicts fundamental chemomechanical phenomena: ligand relaxation softens tangent surface moduli, and adsorption-stress Maxwell relations explicitly link lattice strain to ligand coverage. Applying this theory, we demonstrate that nanostructure behavior is governed by the derivatives of the open-system interfacial free energy and finite-size corrections rather than the scalar energy alone. Open-system residual stress dictates lattice strain; favorable chemical interfacial energy drives core/shell wetting by overpowering positive elastic mismatch; and geometric regularizations, such as curvature, thermodynamically arrest runaway subdivision.

DOI: 10.1103/zmkb-bj63

I. INTRODUCTION

Surface energy is usually introduced as a positive quantity. The typical atomistic picture is that a free crystalline surface disrupts the bulk symmetry: atoms at the surface have altered coordination, electronic structure, charge distribution, and bonding. In this sense, a surface is a defect with its own properties, e.g., energetic cost, mechanical response, among others. At macroscopic length scales, the effect of a surface or an interface is often negligible in the overall response of the body, but at nanometer length scales, the surface-to-volume ratio is large enough that surface energy, residual surface stress, and surface elasticity can dominate mechanical and thermodynamic behavior. This is the starting point of standard continuum surface mechanics: a surface or interface is represented as a zero-thickness energetic entity with properties different from those of the bulk [1–8]. Applications and physical consequences of this idea have ranged from quantum dots and catalysis to self-assembly and phase transformation (among others), cf. Refs. [9–11]. It is also the setting of Gibbsian surface excess thermodynamics, grand-potential formulations for solid surfaces, and coherent-interface thermodynamics under stress [12–14]. The same surface-to-volume logic is central in nanoparticle thermochemistry and phase stability, where calorimetry and size-dependent phase equilibria are used to infer surface excesses [9,15–18]. The same idea appears in nanocrystal shape calculations. Wulff constructions and atomistic or first-principles models assign an excess free energy to each surface or interface and then use those excesses to predict preferred shapes. For ligand-capped nanocrystals, however, those excesses are meaningful only after specifying what is present at the surface: vacuum, bound ligands, solvent, counterions, shell atoms, or some other chemical environment. A "surface energy" for a clean facet and a "surface energy" for a ligand-covered facet are therefore not the same thermodynamic quantity [19–21].

In a careful and insightful study, Calvin *et al.* recently brought this issue into sharp focus by applying dissolution calorimetry to oleate-capped semiconductor quantum dots [22]. The experimental idea is simple. Quantum dots of the same material are prepared in different sizes. Smaller particles have more surface area per mole of inorganic material; we denote this molar surface area by A_m. The particles are dissolved, and the measured dissolution enthalpy is corrected for known contributions from the platform, ligand protonation, and the corresponding bulk material. The result is a corrected molar dissolution enthalpy plotted as a function of A_m.

If the surface atoms made the same thermodynamic contribution as bulk atoms, this corrected dissolution enthalpy would have no systematic dependence on A_m. A size-dependent slope therefore measures an excess enthalpy associated with the surface or interface. If s_H denotes the

[*]Contact author: psharma@uh.edu

slope of corrected dissolution enthalpy versus A_m, Calvin *et al.* define the surface enthalpy of formation as

$$\gamma_{\mathrm{cal}}^{H} = -s_H. \tag{1}$$

Thus a positive slope in the dissolution plot corresponds to a negative surface formation enthalpy. For oleate-capped InP, they report $\gamma_{\mathrm{cal}}^{H} \simeq -3.71\ \mathrm{J\,m^{-2}}$; oleate-capped ZnS, CdS, and PbS also give negative values; oleate-capped CdO is approximately zero; and the InP/ZnS core/shell interface gives an even more negative value, approximately $-10.07\ \mathrm{J\,m^{-2}}$ [22]. Calvin *et al.* also emphasize that their measurement is an enthalpy per area, used as a proxy for a surface free energy, and that it is an average over ligand-covered, quasispherical nanocrystal surfaces rather than a clean-surface cleavage energy.

The apparent paradox disappears once the thermodynamic reference state is made explicit. Let γ_{clean} denote the free energy per unit area required to create a clean solid-vacuum surface of the inorganic material. This is the quantity behind the usual broken-bond intuition. For such a clean surface, broken or weakened bonds generally give

$$\gamma_{\mathrm{clean}} > 0. \tag{2}$$

A ligand-covered surface is different. Surface atoms are not simply under-coordinated; they may be bonded to ligands, counterions, shell atoms, or charge-compensating species. Rather than writing all chemical contributions explicitly at this stage, it is useful to group them into a single ligand-stabilization term and write schematically

$$\Gamma_{s0}^{\mu} = \gamma_{\mathrm{clean}} + \Delta\gamma_{\mathrm{chem}}^{\mu}. \tag{3}$$

Here Γ_{s0}^{μ} is the large-radius, ligand-decorated surface grand-potential value at the chosen temperature and chemical potentials, and $\Delta\gamma_{\mathrm{chem}}^{\mu}$ collects adsorption, passivation, ligand-shell, charge-balance, interfacial-bonding, and chemical-reference contributions. These chemical terms are not abstract bookkeeping. Ligand identity, ligand coverage, metal-carboxylate binding, passivation, ordered ligand shells, and reconstruction are known to affect nanocrystal structure and energetics [23–26].

Equation (3) makes the sign issue transparent. It is possible that

$$\gamma_{\mathrm{clean}} > 0, \quad \Delta\gamma_{\mathrm{chem}}^{\mu} < -\gamma_{\mathrm{clean}}, \quad \Gamma_{s0}^{\mu} < 0. \tag{4}$$

This is not a contradiction. It does not say that a clean cleavage surface has negative energy. It says that the chemically decorated open-system excess can be negative because the chemical stabilization of the surface more than compensates the clean-surface cost.

This distinction has appeared before in discussions of negative surface energy in multicomponent systems. Mathur, Sharma, and Cammarata emphasized that the phrase "negative surface energy" becomes ambiguous when adsorbates or chemical reservoirs are part of the reference state [27], responding in part to earlier atomistic claims of negative surface energies for hydrated alumina [28]. If the reference state is a clean single-component surface in vacuum, positivity is the natural expectation. If the reference state includes adsorbates, ligands, protonation reactions, shell species, counterions, or other chemical reservoirs, the corresponding excess may be positive, zero, or negative. The more precise name for the Calvin *et al.* quantity is therefore a ligand-stabilized surface or interface excess enthalpy; in a free-energy formulation, the corresponding continuum object is a surface or interface grand potential. Related thermodynamic arguments have also appeared in discussions of stable colloidal or nanophase materials, where size distributions or finite-size terms are used to infer interfacial free-energy functions rather than a single constant surface energy [29,30].

A closely related, and older, body of work concerns the thermodynamic stabilization of nanocrystalline alloys against grain growth. Weissmüller proposed that solute segregation can drive the grain-boundary excess free energy toward zero, or below, thereby removing the thermodynamic driving force for coarsening [31]; experiments and alloy-design studies have since pursued this mechanism in detail [32–37]. These treatments regard the internal interface as an open system governed by the Gibbs adsorption equation, exactly as we do here for ligand-covered surfaces. They also retain an ingredient that a fixed-chemical-potential treatment does not. Namely, when the segregating species is drawn from a finite reservoir, the chemical potential acquires an explicit dependence on the net interface area, because adsorption at large area depletes the reservoir. Depletion raises the interfacial excess back toward its bare, positive value as area grows and, when the constrained area potential crosses zero, selects an equilibrium grain size. Ligand-capped nanocrystals are, in this sense, the colloidal counterpart of segregation-stabilized nanocrystalline alloys, and we return to the finite-reservoir effect in Sec. XI C as an additional regularization avenue for the subdivision problem.

In the present work, we take the Calvin *et al.* measurements seriously, but with two qualifications that are essential for the mechanics of surfaces. First, the calorimetric number is an effective average enthalpy over ligand-covered, quasispherical nanocrystal surfaces or interfaces; it is not a unique cleavage energy. It depends on ligand coverage, oxidation state, defect chemistry, dissolution products, ligand protonation corrections, entropy, and the thermochemical reference cycle. Second, even after translating the measured enthalpy into a free-energy or grand-potential proxy, the scalar value of that excess is not the same object as surface stress or surface elasticity. Calling the measured quantity a negative surface energy is therefore defensible only when the reference state is stated clearly and when the distinction between value, first derivative, and second derivative is maintained.

That distinction is already familiar in solid surface mechanics. Shuttleworth's theory and later work on surface stress showed that, for solids, surface free energy and surface stress are not generally identical [4,11,38–42]. Gurtin-Murdoch surface elasticity treats the surface as a coherent lower-dimensional elastic material with its own residual stress and elastic moduli [1,3]. Grand-potential descriptions of solid surfaces, adsorption-strain Maxwell relations, and open versus closed elastic coefficients in multicomponent stressed solids have also been developed in other settings [10,13,43–47]. Coherent-interface thermodynamics under stress provides a related framework for solid-solid interfaces [14]. Curvature-dependent surface theories add surface moments and curvature stiffness [48–50]. Atomistic calculations and ligand-dependent Wulff constructions often use surface energies that already include adsorption or passivation [19–21,26].

The novelty of our work is narrower than any of those established subjects highlighted in the preceding paragraph. While Calvin *et al.* [22] provided a qualitative (conceptual) explanation, we implement a theoretical framework to place their work in an appropriate context *and* highlight what physical insights can be obtained in addition to explaining their experiments. Specifically, we formulate a quantum-dot-specific, chemically resolved, open-system extension of Gurtin-Murdoch surface mechanics. The surface remains a coherent zero-thickness material entity, but the closed surface energy density Γ_s is replaced by a ligand-resolved surface Helmholtz density depending on deformation, surface species, chemical potentials, and (importantly) curvature. Eliminating the surface species at fixed chemical potentials gives a reduced surface grand potential Γ_s^μ. In this construction, the calorimetric excess Γ_{s0}^μ, the residual surface stress, and the surface elastic moduli are respectively a value, a first derivative, and a second derivative of one open-system interfacial thermodynamic potential.

This open-system constitutive viewpoint adds two experimentally relevant consequences to the usual fixed-chemistry surface theory. First, ligand relaxation changes tangent surface moduli through Schur-complement softening, so a surface probed at fixed chemical potential need not have the same elastic constants as the same surface probed at fixed coverage. Second, adsorption-surface-stress Maxwell relations connect strain-controlled changes in ligand coverage to ligand-controlled changes in surface stress. These are not new thermodynamic identities in the abstract; the contribution is to place them inside a reduced Gurtin-Murdoch surface grand potential that can be compared directly with quantum-dot calorimetry, lattice-strain measurements, ligand-coverage data, and surface-stress measurements.

The same formulation also gives a natural language for core/shell wetting and finite-size stability. For a coherent core/shell particle, the elastic penalty from lattice mismatch and the chemical driving force from the core/shell interfacial grand potential are distinct terms in the same thermodynamic balance. A negative InP/ZnS interfacial excess can therefore overcome a positive coherent mismatch penalty without violating elasticity. For a finite-size calorimetric series, curvature, edge and corner energies, ligand packing, electrostatics, particle entropy, atomistic discreteness, and kinetic barriers may all enter beyond the leading area term. These effects are not minor corrections once the leading area coefficient is negative; they are the terms that make the morphology problem well posed.

The purpose of the present paper is to express these statements in a continuum theory that stays close to the notation of standard surface mechanics. We first recall the Gurtin-Murdoch variational framework and the distinction among surface energy, surface stress, and surface elasticity. We then reinterpret the Calvin *et al.* calorimetric coefficient as a chemically decorated excess enthalpy and introduce the corresponding surface or interface grand-potential density. The theory is used to derive open-system surface moduli, adsorption-surface-stress Maxwell relations, second-variation stability conditions, a single-ligand constitutive example, curvature and capillary finite-size corrections, and closed-form applications to spherical quantum-dot strain, coherent core/shell wetting, and finite-size regularization.

Readers familiar with Gurtin-Murdoch surface elasticity may skim Secs. II and III, which fix notation and recall the classical theory; the new material begins in Sec. IV.

II. PRELIMINARIES

To study surface energy and related mechanics, it is necessary to define tensors that live on a surface. We largely follow the classical framework by Gurtin and Murdoch [1] and the more recent tutorial of Mozaffari *et al.* [8]. Bold symbols denote ordinary three-dimensional vectors and tensors, whereas blackboard bold symbols denote surface tensors; in particular, the projection tensor is $\mathbb{P}$, the surface identity is $\mathbb{I}$, the surface first Piola-Kirchhoff stress is $\mathbb{S}$, and the surface second Piola-Kirchhoff stress is $\mathbb{T}$. A body occupies a reference domain Ω_0 with boundary $\partial\Omega_0$. The portion on which surface effects are considered is denoted $S_0 \subset \partial\Omega_0$. A material point is $\boldsymbol{x} \in \Omega_0$, the displacement is $\boldsymbol{u}$, and the deformation is

$$\boldsymbol{y}(\boldsymbol{x}) = \boldsymbol{x} + \boldsymbol{u}(\boldsymbol{x}), \quad \boldsymbol{F} = \nabla \boldsymbol{y} = \boldsymbol{I} + \nabla \boldsymbol{u}. \tag{5}$$

The outward unit normal on S_0 is $\boldsymbol{n}$. The projection tensor onto the tangent plane is

$$\mathbb{P} = \boldsymbol{I} - \boldsymbol{n} \otimes \boldsymbol{n}. \tag{6}$$

The surface identity tensor is the projection of the three-dimensional identity onto the tangent plane. We denote it by $\mathbb{I}$ and write

$$\mathbb{I} := \mathbb{P}\boldsymbol{I}\mathbb{P}. \tag{7}$$

Since $\mathbb{P}^2 = \mathbb{P}$ and $\boldsymbol{I}$ is the three-dimensional identity, $\mathbb{I}$ and $\mathbb{P}$ have the same matrix representation. We nevertheless keep both symbols: $\mathbb{P}$ emphasizes projection from the ambient space to the tangent plane, whereas $\mathbb{I}$ emphasizes the identity acting on tangent vectors and surface tensors.

For any vector field $\boldsymbol{a}$ and tensor field $\boldsymbol{A}$, their surface projections are

$$\boldsymbol{a}^s = \mathbb{P}\boldsymbol{a}, \quad \boldsymbol{A}^s = \mathbb{P}\boldsymbol{A}\mathbb{P}. \tag{8}$$

The surface gradient is

$$\nabla_s \phi = \mathbb{P}\nabla\phi, \quad \nabla_s \boldsymbol{a} = (\nabla \boldsymbol{a})\mathbb{P}. \tag{9}$$

The curvature tensor and mean curvature follow the sign convention

$$\mathbb{L} = -\nabla_s \boldsymbol{n}, \quad \kappa = \tfrac{1}{2}\operatorname{tr}\mathbb{L}. \tag{10}$$

For a sphere of radius R with outward normal, this convention gives

$$\mathbb{L} = -\frac{1}{R}\mathbb{P}, \quad \kappa = -\frac{1}{R}. \tag{11}$$

At small strain,

$$\begin{aligned} \boldsymbol{E} &= \tfrac{1}{2}(\nabla \boldsymbol{u} + \nabla \boldsymbol{u}^T), \\ \boldsymbol{E}_s &= \mathbb{P}\boldsymbol{E}\mathbb{P} \\ &= \tfrac{1}{2}[\mathbb{P}\nabla_s \boldsymbol{u} + (\mathbb{P}\nabla_s \boldsymbol{u})^T]. \end{aligned} \tag{12}$$

The bulk first Piola-Kirchhoff stress is denoted $\boldsymbol{S}$ and the surface first Piola-Kirchhoff stress is denoted $\mathbb{S}$. Both are force measures per referential area, but $\mathbb{S}$ is tangential:

$$\mathbb{S}\boldsymbol{n} = \boldsymbol{0}. \tag{13}$$

The second Piola-Kirchhoff bulk and surface stresses are denoted $\boldsymbol{T}$ and $\mathbb{T}$, respectively.

III. CONVENTIONAL THEORY OF MECHANICS OF SURFACES

We first recall the closed-system Gurtin-Murdoch surface theory in the notation of Sec. II. Consider a deformable body occupying the reference domain $\Omega_0 \subset \mathbb{R}^3$, with boundary

$$\partial\Omega_0 = \partial\Omega_0^u \cup \partial\Omega_0^t, \quad \partial\Omega_0^u \cap \partial\Omega_0^t = \emptyset.$$

The displacement is prescribed as $\boldsymbol{u} = \boldsymbol{u}_0$ on $\partial\Omega_0^u$, and the dead traction $\boldsymbol{t}_0$ is prescribed on $\partial\Omega_0^t$. Let $S_0 \subset \partial\Omega_0^t$ denote the portion of the boundary on which surface elasticity is active. The surface is assumed to be coherent with the underlying bulk: there is no independent surface displacement and no slip between the surface and the bulk. Thus the surface displacement is the trace of the bulk displacement on S_0. If S_0 has a boundary curve, we denote by $\boldsymbol{\nu}$ the outward unit co-normal to ∂S_0 lying in the tangent plane of S_0.

Ignoring body forces and curvature moments, the classical body-plus-surface energy functional is

$$\mathcal{F}_{\mathrm{GM}}[\boldsymbol{u}] = \int_{\Omega_0} \Psi(\nabla\boldsymbol{u})\, dV + \int_{S_0} \Gamma_s(\nabla_s\boldsymbol{u})\, dA - \int_{\partial\Omega_0^t} \boldsymbol{t}_0 \cdot \boldsymbol{u}\, dA. \tag{14}$$

Here Ψ is the bulk strain-energy density per reference volume, and Γ_s is the surface excess energy density per reference area of S_0. Equivalently, one may write $\Gamma_s(\nabla\boldsymbol{u})$, as in the standard Gurtin-Murdoch notation, with the understanding that only the tangential part of the displacement gradient is seen by the zero-thickness surface. We write $\Gamma_s(\nabla_s\boldsymbol{u})$ to make this point explicit.

Let $\boldsymbol{u}$ be an equilibrium displacement and let $\delta\boldsymbol{u}$ be an admissible variation, with

$$\delta\boldsymbol{u} = \boldsymbol{0} \quad \text{on } \partial\Omega_0^u.$$

The first variation is defined by

$$\delta\mathcal{F}_{\mathrm{GM}}[\boldsymbol{u}; \delta\boldsymbol{u}] = \frac{d}{d\varepsilon}\mathcal{F}_{\mathrm{GM}}[\boldsymbol{u} + \varepsilon\delta\boldsymbol{u}]|_{\varepsilon=0}. \tag{15}$$

The bulk and surface first Piola-Kirchhoff stresses conjugate to $\nabla\delta\boldsymbol{u}$ and $\nabla_s\delta\boldsymbol{u}$, respectively, are

$$\boldsymbol{S} = \frac{\partial\Psi}{\partial\nabla\boldsymbol{u}}, \quad \mathbb{S} = \frac{\partial\Gamma_s}{\partial\nabla_s\boldsymbol{u}}. \tag{16}$$

Because $\mathbb{S}$ is a surface tensor, it is tangential in the referential surface argument:

$$\mathbb{S}\boldsymbol{n} = \boldsymbol{0}. \tag{17}$$

Consequently,

$$\mathbb{S} : \nabla\delta\boldsymbol{u} = \mathbb{S} : \nabla_s\delta\boldsymbol{u}. \tag{18}$$

Using (15)–(18), the first variation of (14) is

$$\delta\mathcal{F}_{\mathrm{GM}} = \int_{\Omega_0} \boldsymbol{S} : \nabla\delta\boldsymbol{u}\, dV + \int_{S_0} \mathbb{S} : \nabla_s\delta\boldsymbol{u}\, dA - \int_{\partial\Omega_0^t} \boldsymbol{t}_0 \cdot \delta\boldsymbol{u}\, dA. \tag{19}$$

The volume divergence theorem gives

$$\int_{\Omega_0} \boldsymbol{S} : \nabla\delta\boldsymbol{u}\, dV = -\int_{\Omega_0} \delta\boldsymbol{u} \cdot \operatorname{div}\boldsymbol{S}\, dV + \int_{\partial\Omega_0} \delta\boldsymbol{u} \cdot \boldsymbol{S}\boldsymbol{n}\, dA. \tag{20}$$

Similarly, the surface divergence theorem gives

$$\int_{S_0} \mathbb{S} : \nabla_s\delta\boldsymbol{u}\, dA = -\int_{S_0} \delta\boldsymbol{u} \cdot \operatorname{div}_s\mathbb{S}\, dA + \int_{\partial S_0} \delta\boldsymbol{u} \cdot \mathbb{S}\boldsymbol{\nu}\, dl. \tag{21}$$

Since $\delta\boldsymbol{u} = \boldsymbol{0}$ on $\partial\Omega_0^u$, and since $S_0 \subset \partial\Omega_0^t$, substitution of (20) and (21) into (19) yields

$$\begin{aligned}\delta\mathcal{F}_{\mathrm{GM}} = &-\int_{\Omega_0} \delta\boldsymbol{u} \cdot \operatorname{div}\boldsymbol{S}\, dV + \int_{\partial\Omega_0^t\setminus S_0} \delta\boldsymbol{u} \cdot (\boldsymbol{S}\boldsymbol{n} - \boldsymbol{t}_0)\, dA \\ &+ \int_{S_0} \delta\boldsymbol{u} \cdot (\boldsymbol{S}\boldsymbol{n} - \operatorname{div}_s\mathbb{S} - \boldsymbol{t}_0)\, dA \\ &+ \int_{\partial S_0} \delta\boldsymbol{u} \cdot \mathbb{S}\boldsymbol{\nu}\, dl.\end{aligned} \tag{22}$$

Equilibrium requires

$$\delta\mathcal{F}_{\mathrm{GM}}[\boldsymbol{u}; \delta\boldsymbol{u}] = 0$$

for every admissible variation $\delta\boldsymbol{u}$. Therefore the Euler-Lagrange equations and natural boundary conditions are

$$\operatorname{div}\boldsymbol{S} = \boldsymbol{0} \quad \text{in } \Omega_0, \tag{23a}$$

$$\boldsymbol{S}\boldsymbol{n} = \boldsymbol{t}_0 \quad \text{on } \partial\Omega_0^t \setminus S_0, \tag{23b}$$

$$\boldsymbol{S}\boldsymbol{n} - \operatorname{div}_s\mathbb{S} = \boldsymbol{t}_0 \quad \text{on } S_0, \tag{23c}$$

$$\mathbb{S}\boldsymbol{\nu} = \boldsymbol{0} \quad \text{on } \partial S_0. \tag{23d}$$

If S_0 is a closed surface, the edge condition on ∂S_0 is absent. Surface balance (23c) is the Gurtin-Murdoch traction condition: the bulk traction is balanced not only by the prescribed external traction but also by the surface divergence of the surface stress.

For a frame-indifferent elastic surface, the surface density may be expressed in terms of the surface strain. At finite deformation, the coherent surface deformation gradient is

$$\boldsymbol{F}_s = \boldsymbol{F}\mathbb{P} = (\boldsymbol{I} + \nabla\boldsymbol{u})\mathbb{P}.$$

In the small-strain setting used below,

$$\boldsymbol{E}_s = \mathbb{P}\boldsymbol{E}\mathbb{P}, \quad \boldsymbol{E} = \tfrac{1}{2}(\nabla\boldsymbol{u} + \nabla\boldsymbol{u}^T).$$

Thus we write the surface density as

$$\Gamma_s^*(\boldsymbol{E}_s) = \Gamma_s(\nabla_s\boldsymbol{u}). \tag{24}$$

The surface second Piola-Kirchhoff stress is

$$\mathbb{T} = \frac{\partial\Gamma_s^*}{\partial\boldsymbol{E}_s}. \tag{25}$$

A general small-strain expansion about the reference surface is

$$\Gamma_s^*(\boldsymbol{E}_s) = \Gamma_s^0 + \mathbb{T}_0 : \boldsymbol{E}_s + \tfrac{1}{2}\boldsymbol{E}_s : \mathbb{C}_s : \boldsymbol{E}_s + o(|\boldsymbol{E}_s|^2), \quad (26)$$

where

$$\mathbb{T}_0 = \left.\frac{\partial \Gamma_s^*}{\partial \boldsymbol{E}_s}\right|_{\boldsymbol{E}_s=\boldsymbol{0}}, \quad \mathbb{C}_s = \left.\frac{\partial^2 \Gamma_s^*}{\partial \boldsymbol{E}_s\, \partial \boldsymbol{E}_s}\right|_{\boldsymbol{E}_s=\boldsymbol{0}}.$$

The scalar Γ_s^0 is the reference value of the surface excess energy; $\mathbb{T}_0$ is the residual surface stress; and $\mathbb{C}_s$ is the surface elastic tensor. These are a value, a first derivative, and a second derivative of the surface energy, respectively.

For an isotropic surface, $\mathbb{T}_0 = \tau_0 \mathbb{I}$ and

$$\mathbb{C}_s : \boldsymbol{E}_s = \lambda_0 \operatorname{tr}(\boldsymbol{E}_s)\mathbb{I} + 2\mu_0 \boldsymbol{E}_s, \quad (27)$$

so that

$$\mathbb{T}(\boldsymbol{E}_s) = \tau_0 \mathbb{I} + \lambda_0 \operatorname{tr}(\boldsymbol{E}_s)\mathbb{I} + 2\mu_0 \boldsymbol{E}_s + o(|\boldsymbol{E}_s|). \quad (28)$$

The corresponding surface first Piola-Kirchhoff stress follows from the linearized relation between the first and second surface stress measures:

$$\mathbb{S} = (\mathbb{I} + \mathbb{P}\boldsymbol{\nabla}_s \boldsymbol{u})\mathbb{T} + o(|\boldsymbol{\nabla}_s \boldsymbol{u}|). \quad (29)$$

Combining (28) and (29) gives, to first order,

$$\mathbb{S}(\boldsymbol{\nabla}_s \boldsymbol{u}) = \tau_0 \mathbb{I} + \lambda_0 \operatorname{tr}(\boldsymbol{E}_s)\mathbb{I} + 2\mu_0 \boldsymbol{E}_s + \tau_0 \mathbb{P}\boldsymbol{\nabla}_s \boldsymbol{u} + o(|\boldsymbol{\nabla}_s \boldsymbol{u}|). \quad (30)$$

The Cauchy surface stress has a different linearized form:

$$\begin{aligned} \boldsymbol{\sigma}_s &= \tau_0 \mathbb{I} + \lambda_s \operatorname{tr}(\boldsymbol{E}_s)\mathbb{I} + 2\mu_s \boldsymbol{E}_s, \\ \lambda_s &= \lambda_0 - \tau_0, \quad \mu_s = \mu_0 + \tau_0. \end{aligned} \quad (31)$$

Thus, even in a linearized theory, $\mathbb{S}$, $\mathbb{T}$, and $\boldsymbol{\sigma}_s$ are not interchangeable when the residual surface stress τ_0 is nonzero. This distinction is essential in the present paper because the reference value Γ_s^0, the residual surface stress τ_0, and the surface moduli λ_0, μ_0 play different thermodynamic and mechanical roles.

IV. WHAT THE CALVIN *ET AL.* CALORIMETRIC QUANTITIES REPRESENT

The classical surface functional in Sec. III is written per reference area of a surface $S_0 \subset \partial\Omega_0$. To compare that notation with dissolution calorimetry, we take S_0 to be the ligand-covered surface whose area is used in the experimental size series. If n_{mol} denotes the number of moles of inorganic material in the sample, the molar surface area is

$$A_m = \frac{|S_0|}{n_{\mathrm{mol}}}.$$

At this stage, A_m is a thermochemical descriptor of a family of particles of different sizes, not a virtual change of area in a mechanical boundary-value problem.

Calvin *et al.* measure a corrected molar dissolution enthalpy and plot it against A_m [22]. To leading order, their construction may be idealized as

$$\Delta h_{\mathrm{diss}}^{\mathrm{corr}}(A_m) = \Delta h_{\mathrm{diss}}^{\mathrm{bulk}} + s_H A_m + \mathcal{O}(A_m^2), \quad (32)$$

where s_H is the slope of the corrected dissolution enthalpy with respect to molar surface area. The reported surface enthalpy of formation is the negative of this slope:

$$\gamma_{\mathrm{cal}}^H = -s_H = -\left(\frac{\partial \Delta h_{\mathrm{diss}}^{\mathrm{corr}}}{\partial A_m}\right)_{\mathrm{cycle}}. \quad (33)$$

The subscript "cycle" is a reminder that this derivative is defined by the particular calorimetric reaction cycle used in the experiment, not by a clean cleavage operation. In the Calvin *et al.* measurements, the nanocrystals are dissolved in hydrochloric acid after being deposited on a Teflon support. The measured heat, therefore, has to be corrected for the heat associated with the support platform, for protonation of the oleate ligands to oleic acid, and for the dissolution enthalpy of the corresponding bulk inorganic material [22]. The final dissolved chemical species and the bulk reference state are part of the definition of the thermochemical cycle. With that convention fixed, a positive slope of dissolution enthalpy versus A_m corresponds to a negative surface formation enthalpy.

The superscript H in γ_{cal}^H is intentional. The calorimetric quantity is an enthalpy per area. Calvin *et al.* argue that this enthalpy is a useful proxy for a surface free energy, but the continuum theory below should not require that identification as a matter of definition. In the mechanics problem, the corresponding free-energy object is a surface or interface grand potential. The large-radius, reference-state value of that object is denoted here by Γ_{s0}^{μ}. It is a scalar value of a thermodynamic potential, not a surface stress and not a surface modulus.

A schematic bookkeeping expression for a ligand-covered surface is

$$\begin{aligned} \Gamma_{s0}^{\mu} = \Gamma_{\mathrm{bare}}^0 + \Gamma_{\mathrm{ads}}^0(\{\Theta_\alpha^*\}, T) + \Gamma_{\mathrm{lig}}^0(\{\Theta_\alpha^*\}, T) + \Gamma_{\mathrm{ch}}^0(\{\Theta_\alpha^*\}, T) \\ + \Gamma_{\mathrm{curv}}^0(\mathbb{L}_0, \{\Theta_\alpha^*\}, T) - \sum_\alpha \mu_\alpha \Theta_\alpha^*. \end{aligned} \quad (34)$$

Here Θ_α^* are the equilibrium surface excess densities of the relevant surface species at the specified temperature and chemical potentials, or at the chemical reference state used to define the thermodynamic cycle. The terms in (34) represent, respectively, the bare inorganic surface cost, adsorption or inorganic-ligand bonding, ligand-shell contributions, charge-balance or nonstoichiometry contributions, possible curvature or finite-size terms, and reservoir terms. The decomposition is not meant to imply that these contributions can always be separated experimentally. It is a thermodynamic state-space decomposition showing why a positive bare surface cost can coexist with a negative ligand-stabilized excess:

$$\Gamma_{\mathrm{bare}}^0 > 0, \quad \Gamma_{s0}^{\mu} < 0 \quad \text{is possible.}$$

The calorimetric coefficient γ_{cal}^H is therefore best viewed as an enthalpic estimate of this chemically decorated reference excess, after the thermochemical cycle has been fixed. It is not the cleavage energy of a clean solid-vacuum surface.

Two further observations sharpen this identification. First, at fixed temperature, surface strain, and curvature, the reduced surface grand potential obeys the Gibbs adsorption relation $d\Gamma_s^{\mu} = -\sum_\alpha \Theta_\alpha^*\, d\mu_\alpha$ and is therefore a function of the chemical potentials. The coefficient of reversible configurational work in creating referential area at fixed T, $\{\mu_\alpha\}$, $\boldsymbol{E}_s$, and $\mathbb{L}$ is the value of the appropriate open-system surface potential, $\partial \mathcal{F}_{\mu,s}/\partial A = \Gamma^{\mu}_{s}$, where $\mathcal{F}_{\mu,s}$ denotes the surface contribution to the reduced open-system potential. Second, and more fundamentally, for nanocrystals whose atoms remain registered on a fixed reference lattice throughout the calorimetric measurement process, the referential area of any one particle is never varied: the experiment compares distinct particles of different sizes rather than varying the area of any single surface. The corresponding derivative $d\mathcal{F}_{\mu}/dA$ is therefore not sampled by the dissolution experiment, independently of the fact that the measurement returns an enthalpy rather than a free energy. Neither observation diminishes the value of the data. Both say that the number extracted from the size series is not a direct measurement of reversible open-system area work; it is what this section identifies it to be: a cycle-referenced, ligand-stabilized formation excess, or alternatively an enthalpic proxy for the value Γ^{μ}_{s0} of the open-system interfacial thermodynamics, subject to the equilibrium, entropy, and reservoir caveats discussed in this section.

The same distinction is essential for core/shell particles. Let Ω_c denote the core, $\Omega_{\rm sh}$ the shell, $\Sigma_0 = \partial\Omega_c \cap \partial\Omega_{\rm sh}$ the coherent core/shell interface, and S_0 the exterior shell/ligand surface. The coherent-interface condition is that the displacement is continuous across Σ_0. For a prescribed shell composition and ligand reference state, a schematic continuum free energy is

$$\begin{aligned}\mathcal{F}_{\rm cs}[\boldsymbol{u}_c, \boldsymbol{u}_{\rm sh}] = &\int_{\Omega_c} \Psi_c(\nabla \boldsymbol{u}_c, T)\, dV \\ &+ \int_{\Omega_{\rm sh}} \Psi_{\rm sh}(\nabla \boldsymbol{u}_{\rm sh}; f, T)\, dV \\ &+ \int_{\Sigma_0} \Gamma^{\mu}_{c/{\rm sh}}\, dA + \int_{S_0} \Gamma^{\mu}_{{\rm sh}/\ell}\, dA. \end{aligned} \tag{35}$$

Here f denotes the coherent lattice misfit, $\Gamma^{\mu}_{c/{\rm sh}}$ is the core/shell interfacial grand-potential density, and $\Gamma^{\mu}_{{\rm sh}/\ell}$ is the exterior shell/ligand surface grand-potential density. The positive elastic penalty associated with lattice mismatch appears through $\Psi_{\rm sh}$ and, more generally, through strain dependence of $\Gamma^{\mu}_{c/{\rm sh}}$. A negative interfacial grand potential therefore does not mean that mismatch strain is absent. It means that favorable chemical bonding at the interface may overcompensate the positive coherent elastic penalty for the relevant structure and reference state.

Comparing the core/shell particle with an unshelled ligand-covered core gives the wetting balance used explicitly later. In schematic areal form,

$$\Delta\omega_{\rm wet} = \frac{U_{\rm el}}{A_c} + \Gamma^{\mu}_{c/{\rm sh},0} + \frac{A_S}{A_c}\Gamma^{\mu}_{{\rm sh}/\ell,0} - \Gamma^{\mu}_{c/\ell,0}, \tag{36}$$

where $U_{\rm el}$ is the coherent elastic mismatch energy, A_c is the original core surface area, and A_S is the exterior shell surface area. Wetting is favored when $\Delta\omega_{\rm wet} < 0$. The InP/ZnS calorimetric value reported by Calvin *et al.* enters this balance as an estimate of $\Gamma^{\mu}_{c/{\rm sh},0}$, while the lattice mismatch enters through $U_{\rm el}$. These are distinct terms in the same thermodynamic comparison.

Thus the role of the calorimetric quantity in the present theory is precise: it supplies a chemically decorated scalar excess value. Surface stress, surface elastic moduli, strain-induced ligand redistribution, and wetting stability involve derivatives or finite-size corrections of the corresponding open-system surface or interface thermodynamics. Section V formalizes this statement by replacing the closed Gurtin-Murdoch density Γ_s with a ligand-resolved surface Helmholtz density and its reduced grand potential.

V. CHEMICALLY RESOLVED SURFACE GRAND POTENTIAL

Section IV identified the calorimetric coefficient as a chemically decorated surface or interface excess. We now formulate the corresponding continuum object. The geometric setting is the same as in Sec. III. A body occupies the reference domain Ω_0, and $S_0 \subset \partial\Omega_0$ is the portion of the boundary on which surface energetics are active. The surface is coherent with the underlying bulk, so its displacement is the trace of the bulk displacement on S_0. The new ingredient is not a new surface geometry, but a larger thermodynamic state space.

Let Θ_α denote the surface excess density of species α per reference area of S_0. Depending on the system, these species may represent bound ligands, displaced or adsorbed ions, excess surface atoms, charge-compensating species, solvent-related surface species, or coarse-grained variables describing surface reconstruction. The corresponding chemical potentials are denoted μ_α. In a true reservoir problem, these are imposed by the surrounding solution or vapor. In a calorimetric comparison, they should be understood more broadly as chemical reference potentials fixed by the thermochemical cycle.

The closed-composition Gurtin-Murdoch surface density $\Gamma_s(\nabla_s \boldsymbol{u})$ is replaced by a ligand-resolved surface Helmholtz excess density

$$\widehat{\Gamma}_s = \widehat{\Gamma}_s(\nabla_s \boldsymbol{u}, \mathbb{L}, \{\Theta_\alpha\}, \{\nabla_s\Theta_\alpha\}, T). \tag{37}$$

The hat is used to emphasize that this is the surface Helmholtz density before eliminating the surface species. It is an excess density per reference area of the material surface S_0. A schematic bookkeeping decomposition is

$$\begin{aligned}\widehat{\Gamma}_s = &\,\Gamma_{\rm bare}(\nabla_s \boldsymbol{u}, \mathbb{L}, T) + \Gamma_{\rm ads}(\nabla_s \boldsymbol{u}, \mathbb{L}, \{\Theta_\alpha\}, T) \\ &+ \Gamma_{\rm lig}(\nabla_s \boldsymbol{u}, \mathbb{L}, \{\Theta_\alpha\}, \{\nabla_s\Theta_\alpha\}, T) \\ &+ \Gamma_{\rm ch}(\nabla_s \boldsymbol{u}, \mathbb{L}, \{\Theta_\alpha\}, T). \end{aligned} \tag{38}$$

The terms represent, respectively, the bare inorganic surface cost, adsorption or inorganic-ligand bonding, ligand-shell free energy, and charge-balance or nonstoichiometry contributions. This decomposition is not asserted to be unique or directly separable in an experiment. Its purpose is to specify the thermodynamic state variables and to show where ligand and reservoir effects enter the continuum surface density.

For fixed chemical potentials, the appropriate total potential is

$$\mathcal{F}_\mu[\boldsymbol{u},\{\Theta_\alpha\}] = \int_{\Omega_0}\Psi(\nabla\boldsymbol{u},T)\,dV + \int_{S_0}\Big[\widehat{\Gamma}_s(\nabla_s\boldsymbol{u},\mathbb{L},\{\Theta_\alpha\}, \times\{\nabla_s\Theta_\alpha\},T) - \sum_\alpha \mu_\alpha\Theta_\alpha\Big]dA - \int_{\partial\Omega_0^t}\boldsymbol{t}_0\cdot\boldsymbol{u}\,dA. \tag{39}$$

For simplicity, bulk composition variables have been suppressed. They can be added in the usual way if bulk diffusion or off-stoichiometry is part of the problem. In the quantum-dot applications below, the central open variables are the surface excesses.

The variation with respect to the surface species gives the surface chemical equilibrium equations. For admissible variations $\delta\Theta_\alpha$,

$$\delta_\Theta\mathcal{F}_\mu = 0 \tag{40}$$

implies

$$\frac{\partial\widehat{\Gamma}_s}{\partial\Theta_\alpha} - \mathrm{div}_s\left(\frac{\partial\widehat{\Gamma}_s}{\partial\nabla_s\Theta_\alpha}\right) = \mu_\alpha \quad \text{on } S_0. \tag{41}$$

If no supply of species is prescribed on the boundary curve ∂S_0, the associated natural boundary condition is

$$\frac{\partial\widehat{\Gamma}_s}{\partial\nabla_s\Theta_\alpha}\cdot\boldsymbol{\nu} = 0 \quad \text{on } \partial S_0, \tag{42}$$

where $\boldsymbol{\nu}$ is the outward co-normal to ∂S_0 in the tangent plane of S_0. If ligand-gradient terms are absent, (41) reduces to the local adsorption condition

$$\frac{\partial\widehat{\Gamma}_s}{\partial\Theta_\alpha} = \mu_\alpha. \tag{43}$$

The distinction between frozen coverage and equilibrated coverage is important. If ligand exchange is slow on the time scale of the mechanical process, the coverage fields Θ_α are held fixed, and the relevant surface derivatives are taken at fixed Θ_α. If ligand exchange is fast, or if the surface remains in chemical equilibrium with a reservoir, the coverage fields must be eliminated at fixed μ_α. In the general case with ligand-gradient terms, this elimination is a surface variational problem:

$$\mathcal{F}^\mu_{\mathrm{red}}[\boldsymbol{u}] = \int_{\Omega_0}\Psi(\nabla\boldsymbol{u},T)\,dV + \inf_{\{\Theta_\alpha\}}\int_{S_0}\Big[\widehat{\Gamma}_s(\nabla_s\boldsymbol{u},\mathbb{L},\{\Theta_\alpha\}, \times\{\nabla_s\Theta_\alpha\},T) - \sum_\alpha\mu_\alpha\Theta_\alpha\Big]dA - \int_{\partial\Omega_0^t}\boldsymbol{t}_0\cdot\boldsymbol{u}\,dA. \tag{44}$$

Thus the reduced surface response may be nonlocal along S_0 if gradients of coverage are important.

When ligand-gradient terms are negligible, or when coverage is locally equilibrated and nearly uniform on the length scale of interest, the reduction is pointwise. The surface grand-potential density is then

$$\Gamma_s^\mu(\nabla_s\boldsymbol{u},\mathbb{L};\{\mu_\alpha\},T) = \min_{\{\Theta_\alpha\}}\Big[\widehat{\Gamma}_s(\nabla_s\boldsymbol{u},\mathbb{L},\{\Theta_\alpha\},T) - \sum_\alpha\mu_\alpha\Theta_\alpha\Big]. \tag{45}$$

The minimizing coverage is denoted

$$\Theta_\alpha^* = \Theta_\alpha^*(\nabla_s\boldsymbol{u},\mathbb{L};\{\mu_\beta\},T).$$

The first derivative of this reduced potential has a simple form. Let q denote any mechanical variable, such as a component of $\nabla_s\boldsymbol{u}$, $\boldsymbol{E}_s$, or $\mathbb{L}$. Since the equilibrium coverage satisfies

$$\frac{\partial}{\partial\Theta_\alpha}\left(\widehat{\Gamma}_s - \sum_\beta\mu_\beta\Theta_\beta\right)\bigg|_{\Theta=\Theta^*} = 0,$$

the derivative of Θ_α^* does not contribute to the first derivative of Γ_s^μ. Therefore

$$\frac{\partial\Gamma_s^\mu}{\partial q} = \frac{\partial\widehat{\Gamma}_s}{\partial q}\bigg|_{\Theta_\alpha=\Theta_\alpha^*}. \tag{46}$$

This is the standard envelope property of a minimized thermodynamic potential: first derivatives are evaluated at the relaxed coverage, without adding an explicit term proportional to $\partial\Theta_\alpha^*/\partial q$. The assumption is that the system remains on a stable smooth adsorption branch. If coverage jumps, saturation constraints, or competing adsorption states occur, the derivative may be nonsmooth, and the local formula must be modified. Second derivatives are different: they do contain the relaxation of Θ_α^*, and this is the source of the Schur-complement softening derived in Sec. VI.

Neglecting curvature moments for the moment, the open-system surface first Piola-Kirchhoff stress is

$$\mathbb{S}^\mu = \frac{\partial\Gamma_s^\mu}{\partial\nabla_s\boldsymbol{u}} = \frac{\partial\widehat{\Gamma}_s}{\partial\nabla_s\boldsymbol{u}}\bigg|_{\Theta_\alpha=\Theta_\alpha^*}. \tag{47}$$

The reduced mechanical functional then has the same variational structure as the classical Gurtin-Murdoch functional in Sec. III, with Γ_s replaced by Γ_s^μ. Therefore, in the absence of curvature moments, the leading equilibrium conditions are

$$\mathrm{div}\,\boldsymbol{S} = \boldsymbol{0} \quad \text{in } \Omega_0, \tag{48a}$$

$$\boldsymbol{S}\boldsymbol{n} - \mathrm{div}_s\,\mathbb{S}^\mu = \boldsymbol{t}_0 \quad \text{on } S_0, \tag{48b}$$

together with the ordinary traction condition on $\partial\Omega_0^t\setminus S_0$ and the appropriate edge condition on ∂S_0 when S_0 has a boundary. Thus the open-system theory does not change the leading Gurtin-Murdoch force balance. It changes the constitutive meaning of the surface density and of its derivatives.

If curvature dependence is retained, the surface also carries a moment-like thermodynamic stress

$$\mathbb{M}^\mu = \frac{\partial\Gamma_s^\mu}{\partial\mathbb{L}} = \frac{\partial\widehat{\Gamma}_s}{\partial\mathbb{L}}\bigg|_{\Theta_\alpha=\Theta_\alpha^*}. \tag{49}$$

The corresponding balance law contains additional curvature-gradient, moment, and edge terms, as in Steigmann-Ogden-type surface theories. In the present paper, we use curvature dependence mainly to organize finite-size energetics; the central thermodynamic point is already visible before writing the full moment balance: the scalar value of Γ_s^μ may be negative while its first and second mechanical derivatives remain ordinary constitutive quantities.

The reference value relevant to comparison with calorimetry is

$$\Gamma_{s0}^\mu = \Gamma_s^\mu(\mathbf{0}, \mathbb{L}_0; \{\mu_\alpha\}, T), \tag{50}$$

or the analogous value for an internal interface. For a large nearly planar surface, this is the free-energy counterpart of the ligand-stabilized enthalpic excess estimated by dissolution calorimetry. It is a value of the reduced surface grand potential. The residual surface stress and the surface elastic moduli are different derivatives:

$$\tau_i^\mu = \left.\frac{\partial \Gamma_s^\mu}{\partial \xi_i}\right|_0, \quad C_{ij}^\mu = \left.\frac{\partial^2 \Gamma_s^\mu}{\partial \xi_i\, \partial \xi_j}\right|_0, \tag{51}$$

where ξ_i denotes a surface strain, curvature, or symmetry-adapted mechanical mode. Equations (50) and (51) are the precise mathematical separation needed throughout the rest of the paper: calorimetry estimates a ligand-stabilized scalar excess value, whereas lattice strain, surface stress, surface elasticity, and stability involve first derivatives, second derivatives, or finite-size corrections of the same open-system surface thermodynamics.

The same construction applies to a coherent internal interface. For a core/shell particle, one replaces S_0 by the core/shell interface Σ_0 and uses an interface grand-potential density $\Gamma_{c/\mathrm{sh}}^\mu$; the exterior shell/ligand boundary carries its own density $\Gamma_{\mathrm{sh}/\ell}^\mu$. The displacement is continuous across the coherent interface, while the surface or interface excess variables and chemical reference states may differ. This is the thermodynamic structure behind the wetting balance used later for InP/ZnS core/shell quantum dots.

VI. OPEN-SYSTEM CONSTITUTIVE SPECIFICATION FOR LIGAND-DECORATED SURFACES

The preceding section introduced the reduced surface grand potential Γ_s^μ. We now discuss the constitutive consequences of that reduction. The point is not that the Gurtin-Murdoch balance law is replaced. Once the surface species have been eliminated, the leading mechanical balance has the same form as in Sec. III, with Γ_s replaced by Γ_s^μ, when curvature moments are neglected. The new content is constitutive: the surface stress and surface tangent moduli are derivatives of a grand potential obtained from a surface Helmholtz density by eliminating chemically active surface variables.

Let ξ_i denote a small mechanical surface variable. Depending on the problem, ξ_i may be a component of the surface strain $\boldsymbol{E}_s$, a curvature component, or a symmetry-adapted surface deformation mode. Repeated Latin indices label mechanical modes, and repeated Greek indices label surface species. For the local discussion in this section, define the unrelaxed grand-density

$$\widehat{\omega}_s(\xi, \{\Theta_\alpha\}; \{\mu_\alpha\}, T) = \widehat{\Gamma}_s(\xi, \{\Theta_\alpha\}, T) - \sum_\alpha \mu_\alpha \Theta_\alpha. \tag{52}$$

Curvature and surface-gradient arguments are suppressed in (52) only to keep the notation light; they may be included among the mechanical variables ξ_i or retained as additional state variables.

Choose a homogeneous reference state at fixed temperature and fixed chemical potentials $\{\mu_\alpha\}$. Let

$$\Theta_\alpha^0 = \Theta_\alpha^*(0; \{\mu_\beta\}, T)$$

be the equilibrium coverage in that reference state, and set

$$\eta_\alpha = \Theta_\alpha - \Theta_\alpha^0.$$

Chemical equilibrium at the reference state means

$$\left.\frac{\partial \widehat{\omega}_s}{\partial \Theta_\alpha}\right|_0 = \left.\frac{\partial \widehat{\Gamma}_s}{\partial \Theta_\alpha}\right|_0 - \mu_\alpha = 0. \tag{53}$$

Thus the quadratic expansion of the local unrelaxed grand density contains no term linear in η_α:

$$\widehat{\omega}_s = \omega_0^\mu + \tau_i^\Theta \xi_i + \tfrac{1}{2} C_{ij}^\Theta \xi_i \xi_j + B_i^\alpha \xi_i \eta_\alpha + \tfrac{1}{2}\chi_{\alpha\beta}\eta_\alpha\eta_\beta + o(|\xi|^2 + |\eta|^2). \tag{54}$$

Here

$$\tau_i^\Theta = \left.\frac{\partial \widehat{\omega}_s}{\partial \xi_i}\right|_0 = \left.\frac{\partial \widehat{\Gamma}_s}{\partial \xi_i}\right|_0, \tag{55a}$$

$$C_{ij}^\Theta = \left.\frac{\partial^2 \widehat{\omega}_s}{\partial \xi_i\, \partial \xi_j}\right|_0 = \left.\frac{\partial^2 \widehat{\Gamma}_s}{\partial \xi_i\, \partial \xi_j}\right|_0, \tag{55b}$$

$$B_i^\alpha = \left.\frac{\partial^2 \widehat{\omega}_s}{\partial \xi_i\, \partial \Theta_\alpha}\right|_0 = \left.\frac{\partial^2 \widehat{\Gamma}_s}{\partial \xi_i\, \partial \Theta_\alpha}\right|_0, \tag{55c}$$

$$\chi_{\alpha\beta} = \left.\frac{\partial^2 \widehat{\omega}_s}{\partial \Theta_\alpha\, \partial \Theta_\beta}\right|_0 = \left.\frac{\partial^2 \widehat{\Gamma}_s}{\partial \Theta_\alpha\, \partial \Theta_\beta}\right|_0. \tag{55d}$$

The superscript Θ denotes a frozen-coverage derivative. Matrix $\chi_{\alpha\beta}$ is the local chemical stiffness of the surface species; its inverse is the local adsorption susceptibility. Local chemical stability of the coverage variables requires $\chi_{\alpha\beta}$ to be positive definite on the allowed coverage variations.

If the ligand shell is frozen during the mechanical process, then $\eta_\alpha = 0$ and the tangent surface modulus is simply C_{ij}^Θ. If, instead, the surface remains equilibrated with ligand reservoirs at fixed μ_α, the coverage variables must be eliminated. The stationarity condition with respect to η_α gives

$$0 = \frac{\partial \widehat{\omega}_s}{\partial \eta_\alpha} = B_i^\alpha \xi_i + \chi_{\alpha\beta}\eta_\beta + o(|\xi| + |\eta|), \tag{56}$$

and therefore

$$\eta_\alpha^* = -(\chi^{-1})_{\alpha\beta} B_j^\beta \xi_j + o(|\xi|). \tag{57}$$

Substitution into (54) gives the reduced open-system expansion

$$\Gamma_s^\mu(\xi; \{\mu_\alpha\}, T) = \Gamma_{s0}^\mu + \tau_i^\mu \xi_i + \tfrac{1}{2} C_{ij}^\mu \xi_i \xi_j + o(|\xi|^2), \tag{58}$$

with

$$\tau_i^\mu = \tau_i^\Theta \quad \text{on the chosen equilibrium branch,} \tag{59}$$

and

$$C_{ij}^{\mu} = C_{ij}^{\Theta} - B_i^{\alpha}(\chi^{-1})_{\alpha\beta}B_j^{\beta}. \tag{60}$$

Equation (60) is the Schur complement associated with eliminating the surface species. It is the surface analog of the distinction between open- and closed-system elastic coefficients in stressed multicomponent solids [44–47]. When $\chi_{\alpha\beta}$ is positive definite, the subtracted term is positive semidefinite in the coupled mechanical modes. Thus a surface probed at fixed chemical potential is softer than the same surface probed at fixed coverage, with the largest reduction expected when the adsorption susceptibility is large. This is a constitutive prediction, not a change in the leading traction balance.

The same reduction gives adsorption-stress Maxwell relations. The reduced grand potential satisfies

$$\Theta_{\alpha}^{*} = -\frac{\partial \Gamma_s^{\mu}}{\partial \mu_{\alpha}}, \quad \tau_i^{\mu} = \frac{\partial \Gamma_s^{\mu}}{\partial \xi_i}. \tag{61}$$

Assuming a smooth equilibrium branch, equality of mixed derivatives gives

$$\frac{\partial \tau_i^{\mu}}{\partial \mu_{\alpha}} = -\frac{\partial \Theta_{\alpha}^{*}}{\partial \xi_i}. \tag{62}$$

For strain variables ξ_i, (62) is the ligand-shell version of the adsorption-strain Maxwell relations familiar from solid-surface thermodynamics [10,41]. It says that the change of surface stress caused by changing ligand chemical potential is thermodynamically conjugate to the change of adsorption caused by straining the surface. If ξ_i is a curvature mode, the same identity relates ligand-controlled surface moments to curvature-controlled adsorption.

Equations (60) and (62) are the main constitutive consequences of ligand awareness. A classical fixed-chemistry Gurtin-Murdoch surface can fit a residual stress and a surface modulus once those parameters are supplied. The open-system theory predicts how those quantities change with ligand chemical potential, adsorption susceptibility, strain, and curvature. This is why the scalar calorimetric excess, the residual surface stress, and the surface elastic moduli must be treated as distinct quantities: they are not the same measurement.

VII. CALORIMETRIC EXCESS AND DIFFRACTION-INFERRED SURFACE STRESS

Calvin *et al.* also discuss a second ambiguity in the nanocrystal literature: several diffraction studies have reported negative surface stress, negative surface tension, or negative surface energy, with these terms sometimes used interchangeably [22,51–54]. This conflation in the literature is unfortunate and, in our opinion, unnecessary. For solid surfaces, as several authors have pointed out, surface energy and surface stress are already known to be distinct thermodynamic objects. The purpose of the present section is more specific: to say what this distinction becomes for a ligand-covered, chemically open quantum-dot surface, and to clarify which measurements probe which derivatives of the interfacial thermodynamics.

The calorimetric quantity discussed in Sec. IV is a scalar excess enthalpy per area, used here as an estimate of the corresponding surface or interface grand-potential value. A diffraction measurement is different. Diffraction measures lattice spacings; a surface stress is then inferred only after adopting a mechanical model relating lattice strain to surface tractions. Thus calorimetry and diffraction do not measure the same quantity. They may be governed by the same underlying surface thermodynamics, but they probe different quantities.

In the reference-area notation used here, a locally equilibrated ligand-covered surface has the small-strain expansion

$$\Gamma_s^{\mu,*}(\boldsymbol{E}_s;\{\mu_{\alpha}\},T) = \Gamma_{s0}^{\mu} + \mathbb{T}_0^{\mu} : \boldsymbol{E}_s + \tfrac{1}{2}\boldsymbol{E}_s : \mathbb{C}_s^{\mu} : \boldsymbol{E}_s + o(|\boldsymbol{E}_s|^2). \tag{63}$$

The residual surface stress and the tangent surface elasticity are

$$\mathbb{T}_0^{\mu} = \left.\frac{\partial \Gamma_s^{\mu,*}}{\partial \boldsymbol{E}_s}\right|_{\boldsymbol{E}_s=\boldsymbol{0}}, \quad \mathbb{C}_s^{\mu} = \left.\frac{\partial^2 \Gamma_s^{\mu,*}}{\partial \boldsymbol{E}_s\,\partial \boldsymbol{E}_s}\right|_{\boldsymbol{E}_s=\boldsymbol{0}}. \tag{64}$$

Thus Γ_{s0}^{μ}, $\mathbb{T}_0^{\mu}$, and $\mathbb{C}_s^{\mu}$ are respectively a value, a first derivative, and a second derivative of the reduced surface grand potential. A negative value of the first quantity does not determine the signs of the latter two.

For an isotropic surface,

$$\mathbb{T}_0^{\mu} = \tau_0^{\mu}\mathbb{I}, \quad \mathbb{C}_s^{\mu} : \boldsymbol{E}_s = \lambda_0^{\mu}\,\mathrm{tr}(\boldsymbol{E}_s)\mathbb{I} + 2\mu_0^{\mu}\boldsymbol{E}_s. \tag{65}$$

It is therefore entirely possible to have

$$\Gamma_{s0}^{\mu} < 0, \quad \tau_0^{\mu} > 0,$$
$$\mathbb{C}_s^{\mu}\ \text{positive on the relevant admissible surface-strain modes.} \tag{66}$$

It is also possible to have a compressive residual surface stress while the scalar calorimetric excess is positive. Neither sign implication is thermodynamically valid without additional constitutive information.

The same distinction is often written in current-area notation through a Shuttleworth-type relation. For a solid surface described by a current-area excess γ, the surface stress is commonly expressed as

$$\Upsilon_{ij} = \gamma\delta_{ij} + \frac{\partial \gamma}{\partial \epsilon_{ij}}, \quad i,j = 1,2, \tag{67}$$

with refinements depending on the precise thermodynamic framework and stress measure [4,11,13,38–42]. For a ligand-covered open surface, the derivative must specify the chemical constraint. If the ligand shell is equilibrated with reservoirs, the natural analog is

$$\Upsilon_{ij}^{\mu} = \gamma^{\mu}\delta_{ij} + \left.\frac{\partial \gamma^{\mu}}{\partial \epsilon_{ij}}\right|_{T,\{\mu_{\alpha}\}}. \tag{68}$$

If the ligand shell is frozen during the mechanical process, the derivative is instead taken at fixed coverages:

$$\Upsilon_{ij}^{\Theta} = \gamma^{\Theta}\delta_{ij} + \left.\frac{\partial \gamma^{\Theta}}{\partial \epsilon_{ij}}\right|_{T,\{\Theta_{\alpha}\}}. \tag{69}$$

Equations (68) and (69) are not merely notational variants. They correspond to different experimental protocols. A slowly exchanging ligand shell, a rapidly equilibrating ligand shell, and a calorimetric dissolution cycle need not sample the same derivative of the same interfacial free-energy landscape.

This is the precise sense in which the Calvin *et al.* calorimetric measurement and diffraction-inferred surface-stress measurements should be compared. The calorimetric slope estimates a ligand-stabilized scalar excess value, denoted here by Γ_{s0}^{μ} after translation to a free-energy or grand-potential description. A diffraction-inferred lattice expansion or contraction is controlled by residual surface stress and surface elastic moduli, such as τ_0^{μ}, λ_0^{μ}, and μ_0^{μ}, through a mechanical boundary-value problem. The two measurements are related only after a constitutive model supplies the first and second derivatives of the same open-system surface thermodynamics.

Accordingly, a negative calorimetric surface excess does not imply a negative diffraction-inferred surface stress. Conversely, a negative surface stress inferred from lattice strain does not prove that the scalar surface excess is negative. The connection between the two is not a sign rule; it is the ligand-aware constitutive structure developed in Secs. V and VI, including the Schur-complement softening of surface moduli and the adsorption-surface-stress Maxwell relation. Section VIII turns to a different question: not whether surface stress equals surface energy, but whether a negative scalar surface excess compromises variational stability.

VIII. SECOND VARIATION AND THE STABILITY QUESTION

The apparent paradox of a negative surface energy may be stated as follows: if creating surface area lowers the free energy, why does the material not subdivide indefinitely or create an arbitrarily large area? This concern is explicit in the negative-surface-energy debate and in discussions of thermodynamically stable colloidal or nanophase materials [27–30]. It is also implicit in the Calvin *et al.* discussion: a negative area coefficient favors smaller particles, but the experimentally observed linear size trend cannot continue indefinitely as particles approach molecular-cluster dimensions [22].

There are two different variational questions here. The first is the elastic stability of a prescribed coherent material surface S_0. In that problem, the admissible variations perturb the displacement, surface strain, curvature, and surface species on the same material surface. The stability criterion is the non-negativity of the second variation of the full bulk-plus-surface potential. The scalar reference value of the surface grand potential does not itself enter that second variation.

The second question is morphological or configurational stability: whether the system can lower its thermodynamic potential by creating additional surface area, roughness, facets, edges, corners, or new particles. In that problem, a negative area coefficient can be destabilizing unless higher-order finite-size terms, chemical constraints, bulk elastic costs, electrostatics, particle entropy, atomistic discreteness, or kinetic barriers intervene. The purpose of this section is to separate these two questions.

A. A minimal scalar-coverage model

Consider a locally homogeneous surface patch and let

$$e = \operatorname{tr} \boldsymbol{E}_s \tag{70}$$

be the areal surface strain. Let θ be a scalar coverage variable, in units chosen so that all terms below have dimensions of energy per reference area. A minimal unrelaxed surface grand density at fixed ligand chemical potential μ is

$$\widehat{\omega}_s(e,\theta;\mu) = \gamma_b + \tau_b e + \tfrac{1}{2}k_b e^2 + \theta(\Delta g_0 + ae - \mu) + \tfrac{1}{2}B(\theta-\theta_0)^2. \tag{71}$$

Here $\gamma_b > 0$ is the bare surface cost, τ_b and k_b are bare mechanical coefficients, $\Delta g_0 - \mu$ is the adsorption driving force relative to the ligand reservoir, a couples surface strain to adsorption, and $B > 0$ penalizes changes in coverage.

The equilibrium coverage at fixed e and μ satisfies

$$0 = \frac{\partial \widehat{\omega}_s}{\partial \theta} = \Delta g_0 + ae - \mu + B(\theta - \theta_0), \tag{72}$$

and hence

$$\theta^*(e;\mu) = \theta_0 - \frac{\Delta g_0 + ae - \mu}{B}. \tag{73}$$

Substitution gives the reduced open-system surface grand potential

$$\begin{aligned}\Gamma_s^{\mu}(e) &= \min_{\theta} \widehat{\omega}_s(e,\theta;\mu)\\ &= \gamma_b + \tau_b e + \frac{1}{2}k_b e^2 + \theta_0(\Delta g_0 + ae - \mu)\\ &\quad - \frac{(\Delta g_0 + ae - \mu)^2}{2B}.\end{aligned} \tag{74}$$

At zero strain,

$$\Gamma_{s0}^{\mu} = \Gamma_s^{\mu}(0) = \gamma_b + \theta_0(\Delta g_0 - \mu) - \frac{(\Delta g_0 - \mu)^2}{2B}. \tag{75}$$

This scalar value can be negative even though $\gamma_b > 0$.

The residual surface stress conjugate to e is

$$\tau_0^{\mu} = \left.\frac{\partial \Gamma_s^{\mu}}{\partial e}\right|_{e=0} = \tau_b + a\theta_0 - \frac{a(\Delta g_0 - \mu)}{B}, \tag{76}$$

and the relaxed open-system surface modulus is

$$k_s^{\mu} = \left.\frac{\partial^2 \Gamma_s^{\mu}}{\partial e^2}\right|_{e=0} = k_b - \frac{a^2}{B}. \tag{77}$$

Thus the sign of Γ_{s0}^{μ} is independent of the signs of τ_0^{μ} and k_s^{μ}. The stability condition for homogeneous areal strain in the reduced open system is

$$k_s^{\mu} = k_b - \frac{a^2}{B} > 0, \tag{78}$$

not $\Gamma_{s0}^{\mu} > 0$.

The same conclusion follows from the second variation before eliminating the coverage. At the homogeneous equilibrium state,

$$\delta^2 \widehat{\omega}_s = \frac{1}{2}[\delta e \quad \delta\theta]\begin{bmatrix} k_b & a \\ a & B \end{bmatrix}\begin{bmatrix} \delta e \\ \delta\theta \end{bmatrix}. \tag{79}$$

If the coverage is frozen during the mechanical perturbation, then $\delta\theta = 0$ and the relevant condition is simply $k_b > 0$. If the coverage is allowed to relax locally at fixed chemical potential, eliminating $\delta\theta$ gives the Schur complement $k_b - a^2/B$.

Equivalently, positivity of the full coupled quadratic form requires

$$B > 0, \quad k_b - \frac{a^2}{B} > 0. \tag{80}$$

The constant value Γ^{μ}_{s0} does not enter these second-variation conditions. A surface can therefore have a negative ligand-stabilized reference excess and still be elastically stable.

B. Tensorial second variation

For the full surface theory, the constitutive, or material-Hessian, part of the second variation about a homogeneous equilibrium state has the schematic form

$$\begin{aligned}(\delta^2\mathcal{F}_\mu)_{\rm mat} = (\delta^2\mathcal{F}_{\rm bulk})_{\rm mat} + \frac{1}{2}\int_{S_0} [\delta\boldsymbol{E}_s : \mathsf{A} : \delta\boldsymbol{E}_s \\ + 2\,\delta\boldsymbol{E}_s : \mathsf{B}^\alpha\,\delta\Theta_\alpha + \delta\Theta_\alpha\,\mathsf{C}_{\alpha\beta}\,\delta\Theta_\beta \\ + \mathsf{K}_{\alpha\beta}\,\nabla_s\delta\Theta_\alpha\cdot\nabla_s\delta\Theta_\beta + \delta\mathbb{L} : \mathsf{D} : \delta\mathbb{L} \\ + 2\,\delta\boldsymbol{E}_s : \mathsf{H} : \delta\mathbb{L} + \cdots]\,dA.\end{aligned} \tag{81}$$

Here A is the frozen-coverage surface elastic tensor, B^α is the strain-coverage coupling tensor, $\mathsf{C}_{\alpha\beta}$ is the local chemical stiffness of the surface species, $\mathsf{K}_{\alpha\beta}$ penalizes nonuniform coverage, and D and H collect curvature and strain-curvature terms. The bulk material-Hessian contribution must likewise be positive on the relevant variations. Equation (81) does not, by itself, display the complete displacement second variation about a prestressed state. The latter also contains geometric-stiffness terms generated by first derivatives of the energy, such as $\mathbb{T}^{\mu}_0 : \delta^2\boldsymbol{E}_s$, together with the analogous bulk-prestress contribution and residual-moment terms when curvature is present. It is through these terms that residual surface stress enters the Steigmann-Ogden stability condition. Positivity of the constitutive Hessian, including the Schur complement below, is therefore a material-stability condition rather than a sufficient condition for stability against every admissible displacement perturbation.

If coverage-gradient terms are negligible, elimination of the local coverage variables gives the relaxed open-system surface elasticity tensor in Schur-complement form,

$$\mathbb{C}^{\mu}_s = \mathsf{A} - \mathsf{B}^\alpha(\mathsf{C}^{-1})_{\alpha\beta}\mathsf{B}^\beta, \tag{82}$$

with the obvious interpretation of contractions over the species indices and surface strain indices. If coverage-gradient terms are important, the elimination is no longer pointwise: the inverse in (82) is replaced by the inverse of the corresponding surface differential operator. This gives a nonlocal relaxed surface modulus along S_0.

Equation (82) is the tensorial expression of the same physical point as the scalar model. Ligand relaxation changes the tangent moduli, but the reference value of the surface grand potential is not the criterion for elastic stability. The sign of Γ^{μ}_{s0} is a statement about the value of the open-system excess. Stability is a statement about the second variation of the appropriate bulk-plus-surface potential.

The separation drawn here between the value and its derivatives has an instructive antecedent in the purely mechanical theory. Steigmann and Ogden proved that, for a fixed-chemistry elastic surface without curvature resistance, a negative residual surface stress violates a necessary condition for positivity of the second variation and hence implies instability; this observation was a principal motivation for endowing the surface with curvature elasticity [48,49]. That theorem constrains a *first derivative* of the surface energy. The present analysis makes the complementary point that, for fixed-material elastic variations, the *value*Γ^{μ}_{s0} is left unconstrained by the same stability requirements. The two statements are fully consistent, and they are discussed in Secs. IX and X. Curvature terms regularize the short-wavelength ill-posedness associated, respectively, with negative residual surface stress in the classical theory and with a negative area coefficient in the open-system theory, while stability of all admissible modes remains a quantitative question of material parameters, size, wavelength, and boundary conditions.

C. Morphological area creation

A different question arises when an admissible configurational variation changes the material surface itself, rather than merely deforming a fixed set of surface material points. To isolate this effect, consider a family of interfaces over a fixed projected footprint whose shapes are described by

$$w(x) = a\cos qx. \tag{83}$$

For small slopes,

$$dA \simeq \left(1 + \tfrac{1}{2}|\nabla w|^2\right) dA_p, \quad 2\kappa \simeq -\nabla^2 w, \tag{84}$$

where A_p is the projected area and the sign convention follows Sec. II. The additional area is here understood to be created or recruited configurationally and to equilibrate chemically at the prevailing chemical potentials. Suppose its grand potential also contains a curvature penalty, as in Canham-Helfrich or Steigmann-Ogden-type curvature elasticity [48–50,55,56],

$$\begin{aligned}\Delta\mathcal{F}_{\rm conf}[w] = \Gamma^{\mu}_{s0}(A[w] - A_p) + \frac{1}{2}\int_S B_\kappa(2\kappa)^2\,dA \\ + \Delta\mathcal{F}_{\rm bulk}[w].\end{aligned} \tag{85}$$

Then the leading second-order change per projected area is

$$\frac{\Delta^{(2)}\mathcal{F}_{\rm conf}}{A_p} = \frac{a^2}{4}\left(\Gamma^{\mu}_{s0}q^2 + B_\kappa q^4\right) + \frac{\Delta^{(2)}\mathcal{F}_{\rm bulk}}{A_p}. \tag{86}$$

If $\Gamma^{\mu}_{s0} < 0$, the configurational area term favors creation or recruitment of chemically equilibrated area. A model containing only this area term is then morphologically incomplete. Positive curvature stiffness, edge and corner energies, ligand saturation, finite atomic size, ligand-gradient penalties, electrostatics, particle translational entropy, positive bulk-elastic constraints associated with nonuniform deformation or mismatch, and kinetic barriers are not minor details; they are the terms that make the configurational morphology problem well posed.

This conclusion must not be transferred to elastic corrugation of an existing material surface. For a fixed material surface, the constant value Γ^{μ}_{s0} drops out, and the corresponding q^2 geometric-stiffness term is governed by the residual surface stress; for an isotropic flat reference surface it is $a^2\tau^{\mu}_0 q^2/4$, not $a^2\Gamma^{\mu}_{s0}q^2/4$. Fracture, subdivision, and nucleation of new particles are further configurational changes that create fresh area and may also change topology. Their newly created surfaces need not initially be in the equilibrated ligand state assumed in (85); that distinction is taken up in Sec. VIII D.

Uniform capillary relaxation of the spherical dilation mode discussed later is a different effect. After the homogeneous strain is minimized out, that relaxation lowers the total potential. It is therefore not the stabilizing mechanism that prevents runaway subdivision. This distinction is especially important for quantum dots, because a continuum surface-area expansion cannot remain valid down to arbitrarily small molecular clusters.

D. Fracture and freshly created surface

The analysis of this section concerns variations about a chemically equilibrated, ligand-covered state. Fracture poses a different question: does a negative equilibrated excess bear on crack nucleation or propagation? The theory supplies a clean distinction between a surface that exists in chemical equilibrium and a surface that is being created. Crack advance exposes fresh solid on the time scale of bond rupture; in the fast-fracture limit, adsorption from the surrounding medium cannot equilibrate on the new faces before separation is complete. A crack therefore pays, at the moment of creation, the clean-surface (or at most partially passivated) cost. In the ideal fast-brittle limit, the reversible surface-creation contribution to the fracture resistance is $2\gamma_{\text{clean}} > 0$ of Eq. (2), not the equilibrated excess. The negative open-system value $\Gamma^{\mu}_{s0} < 0$ is attained only after subsequent ligand transport, adsorption, and equilibration; whether that chemistry remains coupled to crack advance depends on the crack velocity relative to transport and adsorption rates. If the crack grows slowly enough that its tip remains in chemical equilibrium with the reservoir, the effective work of separation is reduced from $2\gamma_{\text{clean}}$ toward the equilibrated excess of the two created surfaces, in the manner of the classical thermodynamic treatments of chemically assisted decohesion [57,58] and consistent with stress-corrosion phenomenology. A complete propagation criterion is, of course, kinetic as well as thermodynamic. The criterion compares the mechanical energy-release rate with an environment- and rate-dependent resistance that includes process-zone dissipation and lattice trapping, and subsequent equilibration cannot recover irreversible work already expended. The statements made here bound only the reversible, surface-thermodynamic part of that resistance. In the ideal fully equilibrated and purely brittle limit, a negative excess removes the positive surface-thermodynamic contribution to the Griffith threshold; without, by itself, establishing barrier-free crack nucleation or propagation. Even in that restricted sense, this is not a new paradox. It is the subdivision question of Sec. VIII C expressed in fracture language, and its resolution draws on the same ingredients: transport kinetics, finite ligand supply (Sec. XI C), and the positive nonarea finite-size terms of Sec. X. The latter can regularize or limit the process, though they do not by themselves guarantee arrest of a macroscopically loaded crack. Fracture is thus an application of the framework rather than an exception to it. The theory assigns a chemically starved surface cost to fast crack growth, and a chemically equilibrated one to slow growth, and the paradox lives only in the idealized limit of instantaneous equilibration and vanishing dissipation.

IX. A SINGLE-LIGAND CURVATURE-REGULARIZED CONSTITUTIVE MODEL

The general density $\widehat{\Gamma}_s$ is intentionally broad. To make the ligand-aware constitutive closure operational, consider a single ligand species with maximum site density N_s and fractional coverage

$$0 \leqslant \theta \leqslant 1, \quad \Theta = N_s\theta.$$

This is not intended as a detailed molecular model of oleate chemistry. It is a minimal constitutive example showing how adsorption, surface strain, curvature, and open-system elastic moduli enter one surface grand potential.

Let

$$e = \operatorname{tr}\boldsymbol{E}_s, \quad c = 2(\kappa - \kappa_*), \tag{87}$$

where κ_* is a preferred curvature associated with the ligand-decorated surface. A minimal isotropic Helmholtz excess density is

$$\begin{aligned}\widehat{\Gamma}_s(e, c, \theta) = {} & \gamma_0^B + \tau_0^B e + \tfrac{1}{2}M_B e^2 \\ & + N_s\theta\big(\Delta g_0 + \tau_0^L e + \tfrac{1}{2}M_L e^2\big) \\ & + k_B T N_s[\theta \ln\theta + (1-\theta)\ln(1-\theta)] \\ & + \tfrac{1}{2}B_\kappa(\theta)c^2.\end{aligned} \tag{88}$$

Here $\gamma_0^B > 0$ is the bare clean-surface penalty, Δg_0 is the ligand binding free energy per occupied site, τ_0^L and M_L describe how binding changes under surface strain, the logarithmic term is the ideal lattice-gas mixing free energy underlying the Langmuir isotherm [59], and $B_\kappa(\theta) > 0$ is an effective curvature or ligand-packing modulus.

The reduced surface grand-potential density is

$$\Gamma_s^{\mu}(e, c; \mu) = \min_{0\leqslant\theta\leqslant 1}[\widehat{\Gamma}_s(e, c, \theta) - \mu N_s\theta]. \tag{89}$$

The chemical equilibrium condition is

$$\frac{\partial\widehat{\Gamma}_s}{\partial\theta} = \mu N_s. \tag{90}$$

For the ideal lattice gas, this gives the strain- and curvature-gated isotherm

$$\frac{\theta^*}{1-\theta^*} = \exp\left[\frac{\mu - \Delta g_0 - \tau_0^L e - \frac{1}{2}M_L e^2 - \frac{B'_\kappa(\theta^*)}{2N_s}c^2}{k_B T}\right]. \tag{91}$$

Thus strain and curvature shift ligand coverage, and ligand coverage shifts the mechanical boundary condition. A direct experimental test would be to measure ligand exchange, desorption, or coverage under imposed pressure, strain, or size variation. The same adsorption-strain derivative controls the Maxwell relation in Sec. VI and the ligand dependence of surface stress. A fixed-composition Gurtin-Murdoch surface has no analog of (91).

Let

$$\bar{\theta}(\mu) = \theta^*(0, 0; \mu).$$

At zero strain and zero curvature,

$$\frac{\bar{\theta}}{1-\bar{\theta}} = \exp\left[\frac{\mu - \Delta g_0}{k_B T}\right]. \tag{92}$$

The scalar planar grand-potential value is

$$\Gamma_{s0}^{\mu}(\mu) = \gamma_0^B + N_s\bar{\theta}\,\Delta g_0 + k_B T N_s[\bar{\theta}\ln\bar{\theta} + (1-\bar{\theta})\ln(1-\bar{\theta})] - \mu N_s\bar{\theta}. \tag{93}$$

This value may be negative if ligand binding and the chosen chemical reference state are sufficiently favorable. It is still only a scalar value of the reduced interfacial thermodynamics.

By the envelope theorem, the residual open-system surface stress conjugate to the areal strain is

$$\tau_0^{\mu}(\mu) = \left.\frac{\partial \Gamma_s^{\mu}}{\partial e}\right|_{e=0,c=0} = \tau_0^B + N_s\bar{\theta}(\mu)\tau_0^L. \tag{94}$$

Thus a negative Γ_{s0}^{μ} and a tensile $\tau_0^{\mu} > 0$ can coexist. The coefficient τ_0^L is a material derivative; it should not be assumed universally positive. It can depend on ligand head group, facet, charge state, surface reconstruction, solvent, and chemical reference state. The theory requires no fixed sign.

The open-system dilatational modulus is more revealing. At fixed coverage,

$$M_s^{\Theta} = M_B + N_s\bar{\theta}\,M_L. \tag{95}$$

At fixed ligand chemical potential, relaxation of θ gives

$$M_s^{\mu} = M_s^{\Theta} - \left.\frac{\left[N_s\left(\tau_0^L + M_L e\right)\right]^2}{\partial^2\widehat{\Gamma}_s/\partial\theta^2}\right|_{e=0,c=0,\theta=\bar{\theta}}. \tag{96}$$

For the ideal lattice gas at $c = 0$,

$$\left.\frac{\partial^2\widehat{\Gamma}_s}{\partial\theta^2}\right|_{e=0,c=0,\theta=\bar{\theta}} = \frac{k_B T N_s}{\bar{\theta}(1-\bar{\theta})}. \tag{97}$$

Therefore

$$M_s^{\mu}(\mu) = M_B + N_s\bar{\theta}\,M_L - \frac{N_s\left(\tau_0^L\right)^2}{k_B T}\bar{\theta}(1-\bar{\theta}). \tag{98}$$

If $M_L = 0$, this reduces to

$$M_s^{\mu}(\mu) = M_B - \frac{N_s\left(\tau_0^L\right)^2}{k_B T}\bar{\theta}(1-\bar{\theta}). \tag{99}$$

The factor $\bar{\theta}(1-\bar{\theta})$ is the variance of a Bernoulli occupation variable for a single adsorption site. Equivalently, the ligand-number susceptibility of the ideal surface lattice gas is

$$\frac{\partial(N_s\bar{\theta})}{\partial\mu} = \frac{N_s}{k_B T}\bar{\theta}(1-\bar{\theta}). \tag{100}$$

The Schur-complement softening is therefore a fluctuation–response statement: the open-system surface modulus is reduced by the square of the adsorption-strain coupling multiplied by the adsorption susceptibility. The softening is maximal near half coverage and vanishes for empty or saturated surfaces. This is a sharp physical distinction from ordinary Gurtin-Murdoch mechanics. A classical fixed-surface theory can fit M_s, but it does not predict that the modulus should soften most strongly on the steep part of an adsorption isotherm.

Finally, the curvature term in (88) connects this local constitutive model to finite-size stability. The condition $B_\kappa(\theta) > 0$ penalizes curvature at fixed coverage, while the dependence of B_κ on θ makes adsorption curvature-gated through (91). Thus ligand packing can affect both the local surface modulus and the finite-size corrections needed to regularize a negative area coefficient.

X. CURVATURE CORRECTIONS AND CAPILLARY RELAXATION IN FINITE-SIZE CALORIMETRY

Sections V–IX treated the reduced surface grand potential mainly as a local function of surface strain and ligand coverage. For quantum dots, this is not always enough. Radii of one to a few nanometers are comparable to ligand-shell length scales, facet sizes, and reconstruction lengths. Curvature, edge and corner structure, ligand packing, and the discreteness of surface sites can therefore modify the apparent area coefficient inferred from a finite-size series. The purpose of this section is not to argue that curvature is the primary origin of the negative values reported by Calvin *et al.*; the observed chemical trends point more directly to ligand and interfacial bonding. The point is narrower: once the scalar area coefficient is negative, finite-size corrections are no longer optional bookkeeping. They determine how the continuum expansion remains well posed.

Curvature-dependent surface energy is a natural extension of ordinary surface elasticity and is closely related to the Canham-Helfrich membrane bending and Steigmann-Ogden surface-moment theories [48–50,55,56]. Using the curvature tensor

$$\mathbb{L} = -\nabla_s \boldsymbol{n}, \quad \kappa = \tfrac{1}{2}\operatorname{tr}\mathbb{L},$$

with the sign convention of Sec. II, an isotropic local expansion of the reduced surface grand potential may be written schematically as

$$\Gamma_s^{\mu,*}(\boldsymbol{E}_s,\kappa,K_G) = \Gamma_{s0}^{\mu} + \mathbb{T}_0^{\mu} : \boldsymbol{E}_s + \tfrac{1}{2}\boldsymbol{E}_s : \mathbb{C}_s^{\mu} : \boldsymbol{E}_s + m_0^{\mu}(\kappa-\kappa_*) + \tfrac{1}{2}B_\kappa^{\mu}(2\kappa-2\kappa_*)^2 + \bar{B}_\kappa^{\mu}K_G + \beta^{\mu}\operatorname{tr}(\boldsymbol{E}_s)(\kappa-\kappa_*) + \cdots. \tag{101}$$

Here K_G is the Gaussian curvature, not the bulk modulus; m_0^{μ} is a residual surface-moment coefficient; B_κ^{μ} and $\bar{B}_\kappa^{\mu}$ are curvature moduli; and κ_* is a spontaneous or preferred curvature. For a clean centrosymmetric surface, one might set m_0^{μ} and κ_* to zero. For a ligand-covered nanocrystal, there is no general reason to do so. The ligand shell has an inside and an outside, head groups and tails, steric packing, solvent interactions, charge balance, and possible preferred curvature.

For a spherical or nearly spherical particle, the same information can be organized more transparently as a size expansion for the one-particle excess grand potential:

$$G_{\rm ex}^{(1)}(R) = 4\pi R^2\Gamma_{s0}^{\mu} + 4\pi a_\kappa^{\mu}R + 4\pi b_\kappa^{\mu} + o(1). \tag{102}$$

The coefficient a_κ^{μ} collects terms that scale linearly with radius, including mean-curvature, preferred-curvature, edge, and ligand-packing contributions. The coefficient b_κ^{μ} parametrizes radius-independent terms, including bending, Gaussian curvature, corner, cluster-scale, or discrete ligand-packing contributions. Because of the normalization in (102), their actual radius-independent contribution to the excess grand potential of one closed particle is $4\pi b_\kappa^\mu$. Because our convention gives $\kappa = -1/R$ for a sphere with outward normal, the signs of the curvature contributions are absorbed into the effective coefficients a_κ^μ and b_κ^μ.

Some contributions to b_κ^μ have an exact geometric origin. For a complete sphere with $\kappa_* = 0$, the Willmore-type term gives [56,60]

$$\frac{1}{2}B_\kappa^\mu \int_S (2\kappa)^2 \, dA = 8\pi B_\kappa^\mu. \tag{103}$$

Similarly, Gauss-Bonnet gives [61]

$$\int_S K_G \, dA = 4\pi, \quad \bar{B}_\kappa^\mu \int_S K_G \, dA = 4\pi \bar{B}_\kappa^\mu. \tag{104}$$

Thus a smooth closed spherical particle can acquire a radius-independent energy per component from continuum curvature elasticity alone. Such a term produces no local pressure under uniform rescaling of one perfect sphere, but it contributes an $O(n)$ energy when a fixed amount of material is fragmented into n spheres. This local-versus-global distinction is important for the subdivision question.

For one mole of inorganic material with molar volume V_m, the molar surface area of spherical particles is

$$A_m = \frac{3V_m}{R}. \tag{105}$$

Multiplying (102) by the number of particles per mole gives the molar excess grand potential

$$g_{\mathrm{ex}}(A_m) = \Gamma_{s0}^\mu A_m + \frac{a_\kappa^\mu}{3V_m}A_m^2 + \frac{b_\kappa^\mu}{9V_m^2}A_m^3 + \cdots . \tag{106}$$

If the calorimetric enthalpy is used as a proxy for this free-energy expansion, the same algebra applies to the corresponding enthalpic coefficients. The important point is that a finite-range straight-line fit in A_m need not recover only the large-radius value Γ_{s0}^μ.

There is a second, mechanically distinct, contribution with the same leading A_m^2 scaling. It comes from homogeneous capillary relaxation under residual surface stress. Let the spherical dilation mode be

$$\boldsymbol{u} = \varepsilon r \boldsymbol{e}_r,$$

where ε is the uniform radial strain parameter. Neglecting surface-modulus corrections for the moment, the bulk strain energy and the residual surface-stress work give

$$\Pi(\varepsilon) - 4\pi R^2 \Gamma_{s0}^\mu = 6\pi K_b R^3 \varepsilon^2 + 8\pi R^2 \tau_0^\mu \varepsilon, \tag{107}$$

where K_b is the bulk modulus. Minimization gives

$$\varepsilon_* \simeq -\frac{2\tau_0^\mu}{3K_b R}, \quad \Delta\Pi_{\mathrm{rel}} \simeq -\frac{8\pi R\left(\tau_0^\mu\right)^2}{3K_b}. \tag{108}$$

The sign is worth emphasizing. The stored bulk strain energy is positive, but the surface-stress work is negative and larger in magnitude at the minimum. Eliminating a mechanical degree of freedom must lower the total potential.

Retaining the quadratic surface terms gives the exact result for this homogeneous quadratic mode:

$$\Delta\Pi_{\mathrm{rel}} = -\frac{8\pi R^2\left(\tau_0^\mu\right)^2}{3K_b R + 2\tau_0^\mu + 4\left(\lambda_0^\mu + \mu_0^\mu\right)}, \tag{109}$$

provided the denominator is positive. This denominator is the same stability combination that appears in the spherical-dot calculation in Sec. XI A. In the large-radius limit of (109), the corresponding molar contribution is

$$g_{\mathrm{cap}}^{\mathrm{rel}}(A_m) \simeq -\frac{2\left(\tau_0^\mu\right)^2}{9K_b V_m}A_m^2. \tag{110}$$

Thus, in a local-coefficient approximation, the finite-size formation-excess expansion becomes

$$g_{\mathrm{ex}}^{\mathrm{rel}}(A_m) = \Gamma_{s0}^\mu A_m + \left[\frac{a_\kappa^\mu}{3V_m} - \frac{2\left(\tau_0^\mu\right)^2}{9K_b V_m}\right]A_m^2 + \frac{b_\kappa^\mu}{9V_m^2}A_m^3 + \cdots . \tag{111}$$

The coefficient of A_m^2 therefore contains two conceptually different pieces: curvature, edge, or ligand-packing corrections through a_κ^μ, and a negative capillary-relaxation correction through $(\tau_0^\mu)^2$. Homogeneous capillary relaxation strengthens, rather than cures, the tendency of a negative area coefficient to favor smaller particles. It is not the stabilizing mechanism that prevents runaway subdivision.

The apparent formation excess inferred from a local finite-range slope is

$$\begin{aligned}\gamma_{\mathrm{app}}(A_m) &= \frac{\partial g_{\mathrm{ex}}^{\mathrm{rel}}}{\partial A_m} \\ &= \Gamma_{s0}^\mu + 2\left[\frac{a_\kappa^\mu}{3V_m} - \frac{2\left(\tau_0^\mu\right)^2}{9K_b V_m}\right]A_m + \frac{b_\kappa^\mu}{3V_m^2}A_m^2 + \cdots .\end{aligned} \tag{112}$$

Consequently, a calorimetric line fit over a finite size range does not necessarily measure only the planar or large-radius value Γ_{s0}^μ. Curvature, edge/corner, ligand-packing, and capillary-relaxation terms can all alter the observed slope. If the radius range and precision permit, a nonlinear fit in A_m would be more informative than a single straight-line fit.

The same expansion also clarifies the subdivision problem. Suppose a fixed amount of material initially forming one sphere of radius R_0 is divided into n identical spheres, so that each sphere has radius $R_0 n^{-1/3}$. Equation (102) gives

$$G_{\mathrm{ex}}^{\mathrm{tot}}(n) = 4\pi\Gamma_{s0}^\mu R_0^2 n^{1/3} + 4\pi a_\kappa^\mu R_0 n^{2/3} + 4\pi b_\kappa^\mu n + \cdots . \tag{113}$$

If only the first term were present and $\Gamma_{s0}^\mu < 0$, subdivision would be favored. Positive higher-order finite-size terms can stop this trend. In actual quantum dots, these terms may represent smooth curvature elasticity, faceted edge energies, corner energies, ligand-packing frustration, electronic shell effects, particle translational entropy, finite atomic size, or the breakdown of the continuum description at molecular-cluster dimensions. Section XI C turns this scaling into a closed-form equilibrium-size estimate.

A finite-quantum-dot density-functional or quantum mechanical calculation that explicitly includes the inorganic core, ligands, relaxation, reconstruction, and finite shape already contains curvature, edge, corner, and ligand effects implicitly; such calculations have been used to connect passivation, surface reconstruction, ligand coverage, and nanocrystal shape [19–21,26]. The continuum purpose of coefficients such as Γ_{s0}^{μ}, a_{κ}^{μ}, b_{κ}^{μ}, τ_0^{μ}, and $\mathbb{C}_s^{\mu}$ is therefore interpretive should we wish to place quantum calculations in a thermodynamic/mechanics context. A flat-slab calculation may identify a facet contribution but miss finite-dot edge and curvature corrections. A finite-dot calculation may give the total excess but not separate planar surface energy, adsorption, curvature, edge/corner, and capillary-relaxation effects. Extracting continuum coefficients from atomistics or experiment is useful for the same reason that extracting elastic constants is useful: it permits comparison, extrapolation, and coupling to boundary-value problems outside a single atomistic cell.

For the Calvin *et al.* measurements, curvature dependence is a plausible finite-size correction but probably not the primary origin of the negative sign. The material trends are more naturally explained by ligand and interfacial bonding. Nevertheless, curvature and other nonarea terms are essential to the continuum interpretation of nanometer-scale calorimetry: they modify the apparent finite-range slope and provide the finite-size regularization that a negative area coefficient by itself lacks.

XI. APPLICATIONS AND CONNECTIONS TO EXISTING EXPERIMENTS

The preceding sections identify the thermodynamic structure of the chemically resolved surface theory. We now apply that structure to three simple boundary-value or scaling problems motivated by quantum-dot experiments. The purpose is to show, in closed form, which quantities are controlled by the calorimetric excess values reported by Calvin *et al.*, which quantities are controlled by surface-stress derivatives, and which finite-size terms are needed once the leading area coefficient is allowed to be negative [22].

A. Surface-stress-controlled lattice strain of a spherical quantum dot

Consider an isotropic spherical quantum dot of reference radius R and bulk modulus K_b. Its exterior surface is ligand-covered and chemically equilibrated with reservoirs at chemical potentials $\{\mu_\alpha\}$. We ignore nonspherical shape changes and consider the homogeneous radial displacement

$$\boldsymbol{u} = \varepsilon r\, \boldsymbol{e}_r. \tag{114}$$

The bulk strain is $\boldsymbol{E} = \varepsilon \boldsymbol{I}$ to first order, and the bulk elastic energy is

$$U_b(\varepsilon) = \int_{\Omega_0} \frac{1}{2} K_b (\operatorname{tr}\boldsymbol{E})^2\, dV = 6\pi K_b R^3 \varepsilon^2. \tag{115}$$

On the spherical surface, the exact tangential stretch is $1+\varepsilon$. The surface Green strain is therefore

$$\boldsymbol{E}_s = \tfrac{1}{2}[(1+\varepsilon)^2 - 1]\mathbb{I} = \left(\varepsilon + \tfrac{1}{2}\varepsilon^2\right)\mathbb{I} + o(\varepsilon^2). \tag{116}$$

Use the reduced, chemically resolved surface density at fixed chemical potentials, expanded to second order in $\boldsymbol{E}_s$:

$$\Gamma_s^{\mu,*}(\boldsymbol{E}_s) = \Gamma_{s0}^{\mu} + \tau_0^{\mu} \operatorname{tr}\boldsymbol{E}_s + \frac{\lambda_0^{\mu}}{2}(\operatorname{tr}\boldsymbol{E}_s)^2 + \mu_0^{\mu}\boldsymbol{E}_s : \boldsymbol{E}_s + o(|\boldsymbol{E}_s|^2). \tag{117}$$

Here Γ_{s0}^{μ} is the scalar ligand-stabilized surface excess, τ_0^{μ} is the residual surface stress, and λ_0^{μ}, μ_0^{μ} are open-system surface moduli. Since $\operatorname{tr}\mathbb{I} = 2$ and $\mathbb{I} : \mathbb{I} = 2$,

$$\Gamma_s^{\mu,*}(\varepsilon) = \Gamma_{s0}^{\mu} + 2\tau_0^{\mu}\varepsilon + \left[\tau_0^{\mu} + 2\left(\lambda_0^{\mu} + \mu_0^{\mu}\right)\right]\varepsilon^2 + o(\varepsilon^2). \tag{118}$$

The total potential, up to second order in ε, is

$$\Pi(\varepsilon) = 6\pi K_b R^3 \varepsilon^2 + 4\pi R^2\left\{\Gamma_{s0}^{\mu} + 2\tau_0^{\mu}\varepsilon + \left[\tau_0^{\mu} + 2\left(\lambda_0^{\mu} + \mu_0^{\mu}\right)\right]\varepsilon^2\right\}. \tag{119}$$

Stationarity gives

$$\varepsilon_*(\mu) = -\frac{2\tau_0^{\mu}}{3K_b R + 2\tau_0^{\mu} + 4\left(\lambda_0^{\mu} + \mu_0^{\mu}\right)}, \tag{120}$$

and the homogeneous dilation mode is stable when

$$3K_b R + 2\tau_0^{\mu} + 4\left(\lambda_0^{\mu} + \mu_0^{\mu}\right) > 0. \tag{121}$$

Condition (121) governs this homogeneous dilation mode alone; it is not asserted as sufficient for stability against arbitrary admissible perturbations, which are governed by the tensorial conditions of Sec. VIII B.

The reference value Γ_{s0}^{μ} drops out of both (120) and (121). This is the cleanest closed-form statement of the distinction between calorimetric surface excess and diffraction-inferred lattice strain. Within the present sign convention, a tensile residual surface stress gives a contraction, while a compressive residual surface stress gives an expansion, provided the denominator in (120) is positive. A lattice-spacing measurement therefore probes τ_0^{μ} and the open-system surface moduli, not the sign of Γ_{s0}^{μ} itself.

It is worth recording the large-radius limit of (120), which connects the result to classical solid-state capillarity. When $3K_b R \gg |2\tau_0^{\mu} + 4(\lambda_0^{\mu} + \mu_0^{\mu})|$,

$$\varepsilon_*(\mu) \simeq -\frac{2\tau_0^{\mu}}{3K_b R}, \qquad \bar{\sigma} \equiv 3K_b\varepsilon_* \simeq -\frac{2\tau_0^{\mu}}{R}, \tag{122}$$

where $\bar{\sigma}$ is the mean stress in the particle. This is the generalized capillary equation for solids of Weissmüller and Cahn [62], $\langle\sigma_{kk}\rangle/3 = -\frac{2}{3}f\,(A/V)$, specialized to a single sphere, for which $A/V = 3/R$; the interface stress f is here the open-system residual surface stress $\tau_0^{\mu}(\mu)$, evaluated at the prevailing chemical potentials. The denominator of (120) supplies the surface-elasticity correction to this classical result at finite radius. The agreement is a useful consistency check: the ligand-aware theory reproduces the leading-order large-R limit of established solid-state capillarity, with all of the chemistry absorbed into the value and the derivatives of the reduced surface grand potential.

The algebraic spherical solution is classical Gurtin-Murdoch mechanics. The ligand-aware content is that τ_0^{μ}, λ_0^{μ}, and μ_0^{μ} are not merely fitted constants after chemical equilibration. They are first and second derivatives of the reduced surface grand potential and therefore obey the Schur-complement and adsorption-surface-stress Maxwell relations derived above. A ligand exchange from reservoir state $\mu^{(1)}$ to reservoir state $\mu^{(2)}$ changes the lattice strain by changing these derivatives; it does not act through the scalar calorimetric value Γ^{μ}_{s0} alone.

B. Chemically driven wetting of a strained InP/ZnS core/shell particle

The Calvin *et al.* core/shell measurement is a natural application because it combines a strongly favorable InP/ZnS interfacial excess with a positive lattice-mismatch strain penalty [22]. Core/shell quantum dots are widely used to passivate surfaces and tune optical properties [63,64], and InP-based core/shell particles have been studied explicitly for mismatch strain, shell composition, and shell-thickness effects [65–67]. We idealize the quantum dot as a coherent spherical core of radius R surrounded by an isotropic shell of outer radius

$$a = R + h. \tag{123}$$

The core has bulk modulus K_c, and the shell has bulk and shear moduli K_{sh} and G_{sh}. The shell has an isotropic stress-free misfit strain f relative to the coherent core; only f^2 enters the elastic energy below.

Spherical symmetry gives

$$\boldsymbol{u}_c = Ar\,\boldsymbol{e}_r, \quad \boldsymbol{u}_{\mathrm{sh}} = \left(Br + \frac{C}{r^2}\right)\boldsymbol{e}_r. \tag{124}$$

The core stress is hydrostatic,

$$\sigma^c_{rr} = 3K_cA. \tag{125}$$

In the shell, the elastic strain is the total strain minus $f\boldsymbol{I}$, and hence

$$\sigma^{\mathrm{sh}}_{rr}(r) = 3K_{\mathrm{sh}}(B-f) - 4G_{\mathrm{sh}}\frac{C}{r^3}, \tag{126}$$

$$\sigma^{\mathrm{sh}}_{\theta\theta}(r) = 3K_{\mathrm{sh}}(B-f) + 2G_{\mathrm{sh}}\frac{C}{r^3}. \tag{127}$$

To isolate the positive coherent-misfit energy from the scalar wetting grand potentials, we first set the residual interface and exterior surface stresses to zero. The coherent interface and traction-free exterior then impose

$$AR = BR + \frac{C}{R^2}, \quad \sigma^c_{rr}(R) = \sigma^{\mathrm{sh}}_{rr}(R), \quad \sigma^{\mathrm{sh}}_{rr}(a) = 0. \tag{128}$$

This is a deliberately simplified elastic-wetting calculation, not a claim that the real shell/ligand surface or core/shell interface has zero stress. If the exterior shell/ligand surface has isotropic residual stress $\tau^{\mu}_{\mathrm{sh}/\ell}$, then the last condition is replaced by

$$\sigma^{\mathrm{sh}}_{rr}(a) = -\frac{2\tau^{\mu}_{\mathrm{sh}/\ell}}{a}. \tag{129}$$

Similarly, with the interface normal directed from the core to the shell, an isotropic core/shell interface stress $\tau^{\mu}_{c/\mathrm{sh}}$ changes the coherent interface traction condition to

$$\sigma^{\mathrm{sh}}_{rr}(R) - \sigma^c_{rr}(R) = \frac{2\tau^{\mu}_{c/\mathrm{sh}}}{R}. \tag{130}$$

These terms add ligand-dependent Laplace strains of the same type discussed in the spherical-dot calculation. They are omitted in the algebra below only to keep the competition between coherent mismatch and scalar wetting excesses transparent.

Define

$$q = \left(\frac{R}{a}\right)^3, \quad D = 1 + \frac{4G_{\mathrm{sh}}q}{3K_{\mathrm{sh}}} + \frac{4G_{\mathrm{sh}}(1-q)}{3K_c}. \tag{131}$$

Solving (128) gives

$$C = -\frac{R^3 f}{D}, \tag{132}$$

$$B = f - \frac{4G_{\mathrm{sh}}q}{3K_{\mathrm{sh}}}\frac{f}{D}, \tag{133}$$

$$A = \frac{4G_{\mathrm{sh}}(1-q)}{3K_c}\frac{f}{D}. \tag{134}$$

The elastic strain energy is obtained by integrating the quadratic elastic energy density in the core and shell. The core contribution is $6\pi K_cR^3A^2$. In the shell, with $Y = B - f$,

$$U_{\mathrm{sh}} = 6\pi K_{\mathrm{sh}}Y^2(a^3 - R^3) + 8\pi G_{\mathrm{sh}}C^2(R^{-3} - a^{-3}). \tag{135}$$

Using (132)–(134), the total coherent misfit energy collapses to

$$U_{\mathrm{el}}(R, h, f) = \frac{8\pi G_{\mathrm{sh}}R^3(1-q)f^2}{D}. \tag{136}$$

Since K_c, K_{sh}, and G_{sh} are positive, $D > 0$ and $U_{\mathrm{el}} > 0$ for $h > 0$ and $f \neq 0$.

Now compare the core/shell particle with an unshelled ligand-covered core. The grand-potential change associated with replacing the core/ligand surface by a coherent core/shell interface plus a ligand-covered shell exterior is

$$\Delta\Omega_{\mathrm{wet}}(h) = U_{\mathrm{el}}(R, h, f) + 4\pi R^2\Gamma^{\mu}_{c/\mathrm{sh}} + 4\pi a^2\Gamma^{\mu}_{\mathrm{sh}/\ell} - 4\pi R^2\Gamma^{\mu}_{c/\ell}. \tag{137}$$

Wetting is thermodynamically favored when

$$\Delta\Omega_{\mathrm{wet}}(h) < 0. \tag{138}$$

Per unit original core area,

$$\Delta\omega_{\mathrm{wet}}(h) = \Gamma^{\mu}_{c/\mathrm{sh}} - \Gamma^{\mu}_{c/\ell} + q^{-2/3}\Gamma^{\mu}_{\mathrm{sh}/\ell} + \frac{2G_{\mathrm{sh}}R(1-q)f^2}{D}. \tag{139}$$

For a thin shell, $h/R \ll 1$,

$$\Delta\omega_{\mathrm{wet}}(h) = \Delta\Gamma^{\mu}_0 + h\left[\frac{2\Gamma^{\mu}_{\mathrm{sh}/\ell}}{R} + M_{\mathrm{eff}}f^2\right] + O(h^2/R^2), \tag{140}$$

where

$$\Delta\Gamma^{\mu}_0 = \Gamma^{\mu}_{c/\mathrm{sh}} + \Gamma^{\mu}_{\mathrm{sh}/\ell} - \Gamma^{\mu}_{c/\ell}, \quad M_{\mathrm{eff}} = \frac{6G_{\mathrm{sh}}}{1 + 4G_{\mathrm{sh}}/(3K_{\mathrm{sh}})}. \tag{141}$$

If the bracket in (140) is positive, the thickness at which the positive incremental penalty would offset the initial chemical wetting drive is

$$h_c = -\frac{\Delta\Gamma_0^\mu}{2\Gamma_{\mathrm{sh}/\ell}^\mu/R + M_{\mathrm{eff}} f^2}. \tag{142}$$

If the denominator is negative, this minimal model predicts no finite thermodynamic thickness cutoff; other ingredients such as precursor chemical potentials, nonuniform shelling, finite ligand supply, surface stress, dislocations, facets, or kinetics must then set the observed shell thickness.

For the InP/ZnS system, taking the reported enthalpic excesses as proxies for the corresponding grand-potential values gives

$$\Gamma_{\mathrm{InP}/\ell}^\mu \simeq -3.71\ \mathrm{J\,m^{-2}}, \quad \Gamma_{\mathrm{ZnS}/\ell}^\mu \simeq -1.41\ \mathrm{J\,m^{-2}},$$
$$\Gamma_{\mathrm{InP/ZnS}}^\mu \simeq -10.07\ \mathrm{J\,m^{-2}}. \tag{143}$$

Thus

$$\Delta\Gamma_0^\mu \simeq -10.07 - 1.41 + 3.71 = -7.77\ \mathrm{J\,m^{-2}}. \tag{144}$$

This is a large negative chemical wetting drive. A representative coherent elastic penalty scale,

$$M_{\mathrm{eff}} f^2 h, \tag{145}$$

with $f \simeq 0.08$, $h \simeq 0.807$ nm, and $M_{\mathrm{eff}} \simeq 117$ GPa is about

$$M_{\mathrm{eff}} f^2 h \simeq 0.61\ \mathrm{J\,m^{-2}}, \tag{146}$$

substantially smaller than $|\Delta\Gamma_0^\mu|$. The precise numerical value depends on the shell modulus, misfit definition, shell thickness, relaxation, interfacial stoichiometry, and whether the calorimetric enthalpies are accurate free-energy proxies. The robust conclusion is more important than the particular parameter choice: a large negative interfacial grand potential can overwhelm a positive coherent elastic mismatch penalty without violating elasticity.

To visualize this scale separation, we use the reported InP/oleate, ZnS/oleate, and InP/ZnS excess enthalpies as proxies for the corresponding open-system surface and interface grand-potential values. The leading thin-shell wetting balance may be written as

$$\Delta\omega_{\mathrm{wet}} = \Delta\Gamma_0^\mu + M_{\mathrm{eff}} f^2 h,$$
$$\Delta\Gamma_0^\mu = \Gamma_{\mathrm{InP/ZnS}}^\mu + \Gamma_{\mathrm{ZnS}/\ell}^\mu - \Gamma_{\mathrm{InP}/\ell}^\mu.$$

Figure 1 compares the three chemical/interface terms with a representative coherent elastic mismatch penalty. The figure should be read as an areal wetting balance: the fourth bar is the sum of the first three bars, and the final bar is the sum after adding the elastic penalty.

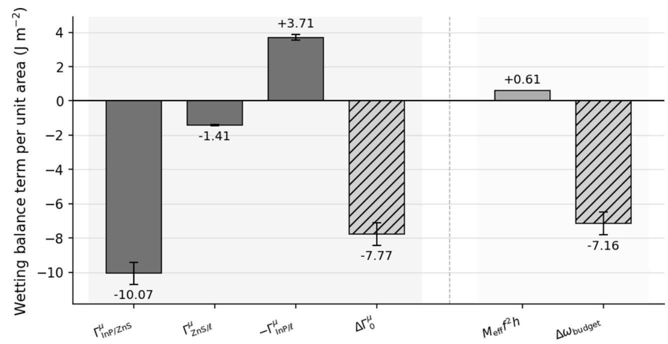

FIG. 1. Areal terms in the leading thin-shell wetting balance for an InP/ZnS core/shell quantum dot. All quantities are normalized by the initial InP core surface area, $A_c = 4\pi R^2$. Negative values favor shell formation; positive values oppose shell formation. The first three bars are the chemical/interface terms in $\Delta\Gamma_0^\mu = \Gamma_{\mathrm{InP/ZnS}}^\mu + \Gamma_{\mathrm{ZnS}/\ell}^\mu - \Gamma_{\mathrm{InP}/\ell}^\mu$. The fourth bar, $\Delta\Gamma_0^\mu = -7.77\ \mathrm{J\,m^{-2}}$, is the sum of these three terms and is not an additional independent measurement. The fifth bar is a representative coherent elastic mismatch penalty, $M_{\mathrm{eff}} f^2 h = +0.61\ \mathrm{J\,m^{-2}}$, computed using $f = 0.08$, $h = 0.807$ nm, and $M_{\mathrm{eff}} = 117$ GPa. The final bar is the resulting net leading-order wetting balance, $\Delta\omega_{\mathrm{wet}} = \Delta\Gamma_0^\mu + M_{\mathrm{eff}} f^2 h = -7.16\ \mathrm{J\,m^{-2}}$. Thus, even after including a representative coherent elastic penalty, favorable InP/ZnS interfacial chemistry overwhelms the positive lattice-mismatch cost. The calorimetric enthalpies from Calvin *et al.* are used here as proxies for surface/interface grand-potential values, and the elastic term is a scale estimate rather than a fitted parameter.

C. Finite-size calorimetry and regularization of a negative area coefficient

Calvin *et al.* note that a linear negative surface-energy trend cannot continue indefinitely as particles approach molecular-cluster dimensions [22]. That observation is not a side issue; it is required for thermodynamic consistency. A negative area coefficient can favor smaller particles, but a continuum theory that contains only a term proportional to surface area is morphologically incomplete. Stable colloidal size distributions, thermodynamically stable nanophases, and magic-sized semiconductor clusters all require physics beyond a single constant area coefficient [18,29,30,68,69].

The finite-size expansion derived in Sec. X can be written for one relaxed spherical particle as

$$G_{\mathrm{ex}}^{(1),\mathrm{rel}}(R) = 4\pi\left[\Gamma_{s0}^\mu R^2 + a_{\mathrm{eff}} R + b\right] + o(1). \tag{147}$$

Here Γ_{s0}^μ is the large-radius area coefficient. Coefficient a_{eff} collects mean-curvature, edge, spontaneous-curvature, ligand-packing, and other $O(R)$ terms, together with the negative homogeneous capillary-relaxation contribution when the simple spherical dilation mode is applicable:

$$a_{\mathrm{eff}} = a_\kappa^\mu - \frac{2\left(\tau_0^\mu\right)^2}{3K_b} + \cdots. \tag{148}$$

The coefficient b parametrizes radius-independent terms such as bending, Gaussian-curvature, corner, electronic-shell, ligand-saturation, or cluster-scale discreteness contributions. With the normalization in (147), the actual radius-independent contribution to the excess grand potential of one closed particle is $4\pi b$. These contributions need not be uniquely separable in experiment. The point is that they are the next terms in the size expansion after the area contribution.

For one mole of inorganic material with molar volume V_m, the molar surface area of spherical particles is

$$A_m = \frac{3V_m}{R}. \tag{149}$$

Equation (147) is equivalent to the molar expansion

$$g_{\mathrm{ex}}^{\mathrm{rel}}(A_m) = \Gamma_{s0}^{\mu} A_m + \frac{a_{\mathrm{eff}}}{3V_m} A_m^2 + \frac{b}{9V_m^2} A_m^3 + \cdots . \tag{150}$$

If the calorimetric enthalpy is used as a proxy for this free-energy expansion, the same algebra applies to the corresponding enthalpic coefficients. A straight-line fit over a finite measured window therefore estimates an apparent slope, not necessarily the asymptotic large-radius value Γ_{s0}^{μ} alone.

The same expansion gives a simple regularization criterion. Take a fixed amount of inorganic material whose volume equals that of one sphere of radius R_0. If it is divided into n equal spheres, each sphere has radius

$$R_n = R_0 n^{-1/3}. \tag{151}$$

The total excess grand potential is

$$G_{\mathrm{ex}}^{\mathrm{tot}}(n) = 4\pi \big[\Gamma_{s0}^{\mu} R_0^2 n^{1/3} + a_{\mathrm{eff}} R_0 n^{2/3} + bn\big]. \tag{152}$$

Let

$$y = n^{1/3}, \quad y \geqslant 1. \tag{153}$$

Then

$$G_{\mathrm{ex}}^{\mathrm{tot}}(y) = 4\pi \big[\Gamma_{s0}^{\mu} R_0^2 y + a_{\mathrm{eff}} R_0 y^2 + by^3\big]. \tag{154}$$

If $a_{\mathrm{eff}} > 0$ and b is negligible, the positive A_m^2 term alone can regularize the negative area coefficient, giving the stationary radius

$$R_* = \frac{2a_{\mathrm{eff}}}{|\Gamma_{s0}^{\mu}|}. \tag{155}$$

More generally, if $b > 0$, stationarity gives

$$3by^2 + 2a_{\mathrm{eff}} R_0 y + \Gamma_{s0}^{\mu} R_0^2 = 0. \tag{156}$$

For $\Gamma_{s0}^{\mu} < 0$, the stable stationary point is

$$y_* = \frac{R_0\big[-a_{\mathrm{eff}} + \sqrt{a_{\mathrm{eff}}^2 - 3b\Gamma_{s0}^{\mu}}\big]}{3b}, \quad n_* = y_*^3, \tag{157}$$

provided $y_* > 1$. The corresponding particle radius is independent of the initial amount of material:

$$R_* = \frac{a_{\mathrm{eff}} + \sqrt{a_{\mathrm{eff}}^2 - 3b\Gamma_{s0}^{\mu}}}{-\Gamma_{s0}^{\mu}}. \tag{158}$$

The second derivative at the stationary point is

$$\left.\frac{d^2 G_{\mathrm{ex}}^{\mathrm{tot}}}{dy^2}\right|_{y_*} = 8\pi R_0 \sqrt{a_{\mathrm{eff}}^2 - 3b\Gamma_{s0}^{\mu}} > 0, \tag{159}$$

so the stationary point is a true minimum within the model.

A particularly transparent limiting case is $a_{\mathrm{eff}} = 0$. Then

$$R_* = \sqrt{\frac{3b}{|\Gamma_{s0}^{\mu}|}}, \quad b = \frac{|\Gamma_{s0}^{\mu}| R_*^2}{3}. \tag{160}$$

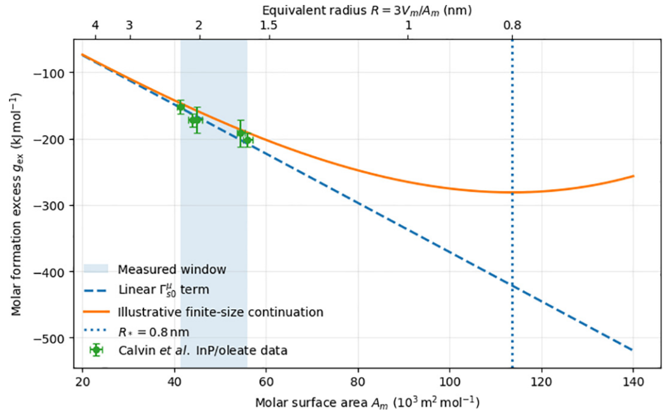

FIG. 2. Finite-size continuation of the InP/oleate calorimetric trend. The horizontal axis is the molar surface area A_m, with the corresponding spherical equivalent radius $R = 3V_m/A_m$ shown on the upper axis. The dashed line is the purely linear area term $g_{\mathrm{ex}} = \Gamma_{s0}^{\mu} A_m$, using the Calvin *et al.* InP/oleate value $\Gamma_{s0}^{\mu} \simeq -3.71\ \mathrm{J\,m^{-2}}$ as an enthalpic proxy for the surface grand-potential coefficient. The green points are the Calvin *et al.* InP dissolution-calorimetry data transformed to the formation-excess convention, $g_{\mathrm{ex}} = -(\Delta h_{\mathrm{diss}} - \Delta h_{\mathrm{diss}}^{\mathrm{bulk}})$. The shaded band marks the measured size window. The solid curve is an illustrative regularized continuation, $g_{\mathrm{ex}}(A_m) = \Gamma_{s0}^{\mu} A_m + bA_m^3/(9V_m^2)$, with $a_{\mathrm{eff}} = 0$ and $b = |\Gamma_{s0}^{\mu}| R_*^2/3$, chosen here so that the minimum occurs at $R_* = 0.8$ nm. The curve is not a fit. Its purpose is to show how a positive nonarea finite-size coefficient can agree with an approximately linear negative-area trend over the measured window while preventing indefinite descent as the particle approaches molecular-cluster dimensions.

Using the InP/oleate value $|\Gamma_{s0}^{\mu}| \simeq 3.71\ \mathrm{J\,m^{-2}}$ as an enthalpic proxy, and choosing an illustrative arrest radius

$$R_* = 0.8\ \mathrm{nm},$$

gives

$$b = \frac{|\Gamma_{s0}^{\mu}| R_*^2}{3} \simeq 7.9 \times 10^{-19}\ \mathrm{J} \simeq 4.9\ \mathrm{eV}. \tag{161}$$

This number should not be interpreted as a fitted parameter. It is the coefficient b inside the overall 4π normalization of (147). The actual radius-independent contribution to the one-particle excess grand potential is therefore $4\pi b \simeq 9.9 \times 10^{-18}$ J $\simeq 62$ eV per closed nanocrystal. Within the deliberately minimal $a_{\mathrm{eff}} = 0$ model, this is the constant contribution required to bend the negative area law over near $R_* = 0.8$ nm. Choosing a different illustrative arrest radius changes b, and hence $4\pi b$, quadratically. The point of the estimate is therefore not the particular value of R_*, but the scale of the nonarea correction needed as the continuum description approaches molecular-cluster dimensions.

Figure 2 shows the corresponding illustrative finite-size continuation. This example converts the qualitative finite-size statement into a continuum criterion. A negative area coefficient can favor small particles, but a positive nonarea correction can produce a stable radius and prevent runaway subdivision. The model should not be read as a complete atomistic theory of magic-sized clusters. At radii approaching the molecular-cluster regime, stoichiometry, faceting, reconstruction, ligand coverage, precursor chemical potentials, and kinetic pathways may dominate. The continuum expansion is useful because it identifies which kind of term is missing from a purely linear area law and how large such a term must be.

The regularization just described operates at fixed chemical potentials: the reservoir is implicitly infinite. If the ligand is instead drawn from a finite inventory, μ falls as the net surface area grows; and since $\partial\Gamma^{\mu}_{s0}/\partial\mu = -\Theta^{*} < 0$ at positive coverage, Eq. (61), the area coefficient $\Gamma^{\mu}_{s0}(\mu)$ rises toward its bare, positive, clean-surface value as subdivision proceeds. Reservoir depletion is therefore a regularization mechanism in its own right and one that operates even in the absence of curvature and discreteness terms, and that selects an equilibrium size when the constrained area potential crosses zero. Equivalently: with a finite total inventory $N_L^{\mathrm{tot}} = N_L^{\mathrm{res}} + A\Theta$, the reservoir chemical potential becomes area-dependent, and at an interior equilibrium the constrained-area derivative of the total potential, which is the closed-system counterpart of a surface tension, vanishes even though the fixed-μ excess evaluated at the initial state is negative. This open-versus closed-system distinction is drawn with particular clarity in the alloy-design literature [34–36]. It is precisely the mechanism underlying the thermodynamic stabilization of nanocrystalline alloys by grain-boundary segregation from a finite solute inventory [31–37].

The finite-size interpretation is also a warning about calorimetric slopes. Over the measured InP window, a linear fit may be an excellent empirical summary. Outside that window, however, the continuation must eventually deviate if the leading area coefficient is negative. Curvature, edge/corner, ligand-packing, electrostatic, particle-entropic, atomistic, or kinetic terms are not decorative corrections in this regime. They are the terms that determine how the negative area coefficient is regularized.

XII. CONCLUDING REMARKS

Negative calorimetric surface and interface excesses reported for ligand-capped quantum dots do not contradict continuum surface mechanics. They contradict only the overgeneralized statement that every chemically specified scalar surface excess must be positive. A clean, solid-vacuum surface energy may remain positive while a ligand-stabilized surface or interface grand potential is negative.

The appropriate continuum object is therefore not merely a constant capillary coefficient. It is a chemically resolved surface density on S_0 depending on $\boldsymbol{\nabla}_s\boldsymbol{u}, \boldsymbol{E}_s$, ligand coverages Θ_α, chemical potentials μ_α, and possibly curvature $\mathbb{L}$. In the absence of curvature moments, the balance equation remains the Gurtin-Murdoch surface balance $\boldsymbol{Sn} - \mathrm{div}_s\,\mathbb{S} = \boldsymbol{t}_0$. What changes is the constitutive interpretation of Γ_s.

The stability issue is well-illustrated by an appeal to a simple variational argument. A negative reference value Γ^{μ}_{s0} is compatible with stability if the relevant second variation is positive. In the chemically resolved theory, coverage relaxation modifies surface elastic tangents through Schur complements and produces Maxwell relations between adsorption and surface stress. In morphology problems, a negative area term alone is incomplete and must be regularized by curvature, edge/corner, ligand-saturation, atomistic, electrostatic, particle-translational-entropic, positive noncapillary bulk-elastic, or kinetic terms. Homogeneous capillary relaxation has the opposite sign after minimization and should not be counted as the regularizer.

We present several closed-form examples to illustrate how the developed theory in this paper can be used. The spherical-quantum dot strain problem shows that ligand-dependent lattice strain is governed by residual surface stress and surface elastic moduli, while Γ^{μ}_{s0} drops out. The coherent core/shell problem shows how a negative chemical interfacial grand potential can be placed quantitatively in competition with positive lattice-mismatch strain; with the PNAS InP/ZnS values, the chemical wetting drive is much larger than a typical nanometer-shell elastic penalty. The finite-size regularization problem shows how curvature, edge, corner, ligand-packing, or cluster corrections can produce a stable radius even when the leading area coefficient is negative; the capillary strain of a spherical particle lowers the relaxed free energy and therefore strengthens, rather than cures, the need for those positive finite-size terms.

Curvature dependence can have real consequences for quantum dots. It changes the relation between calorimetric slope and planar interfacial energy, and it supplies finite-size regularization. Finite quantum-dot quantum calculations already contain curvature and edge effects implicitly, but separating those effects into continuum coefficients is useful for interpretation, extrapolation, comparison with calorimetry, and coupling to surface stress measurements.

ACKNOWLEDGMENTS

The author is grateful to the three anonymous referees for their unusually thorough and constructive reports. In particular, the discussion of segregation-stabilized nanocrystalline alloys and the finite-reservoir mechanism (Sec. XI C), the fixed-reference-lattice argument of Sec. IV, the verification against the Weissmüller-Cahn capillary equation (Sec. XI A), the fracture discussion of Sec. VIII D, and the explicit statement of the Steigmann-Ogden second-variation theorem (Sec. VIII B) were prompted by their comments.

Artificial-intelligence disclosure (per APS policy). A large language model (Anthropic's Claude) was used to create Python code, run on Google Colab, to produce Figs. 1 and 2. Claude and OpenAI models were also used to edit grammar, check for typographical errors, and provide critical feedback on the manuscript. The author takes full responsibility for the content of this paper.

DATA AVAILABILITY

The experimental data analyzed in this work are available in Ref. [22]. The numerical inputs used to generate Figs. 1 and 2 are provided in Tables I–III; the figures can be reproduced directly from the equations and numerical inputs presented in the article. No new experimental data were generated.

APPENDIX: NUMERICAL VALUES USED IN FIGS. 1 AND 2

This Appendix summarizes the numerical inputs used to construct Figs. 1 and 2. Table I lists the calorimetric and interfacial quantities entering Fig. 1, Table II lists the corresponding elastic quantities entering Fig. 1, and Table III lists the illustrative material and thermodynamic parameters entering Fig. 2.

TABLE I. Values used for the calorimetric/interface part of the leading thin-shell InP/ZnS wetting-balance figure. The plotted balance is $\Delta\omega_{\rm wet} = \Delta\Gamma_0^\mu + M_{\rm eff} f^2 h$, with $\Delta\Gamma_0^\mu = \Gamma^\mu_{\rm InP/ZnS} + \Gamma^\mu_{{\rm ZnS}/\ell} - \Gamma^\mu_{{\rm InP}/\ell}$.

Quantity	Value used	Dimensions	Source	Explanation
$\Gamma^\mu_{\rm InP/ZnS}$	-10.07 ± 0.64	$\mathrm{J\,m^{-2}}$	From Calvin *et al.*	Reported InP/ZnS interfacial formation excess from the core/shell calorimetric analysis. Used here as the proxy for the InP/ZnS interfacial grand-potential value.
$\Gamma^\mu_{{\rm ZnS}/\ell}$	-1.41 ± 0.03	$\mathrm{J\,m^{-2}}$	From Calvin *et al.*	Reported ZnS/oleate surface formation excess. Used here as the proxy for the exterior ZnS/ligand surface grand-potential value.
$\Gamma^\mu_{{\rm InP}/\ell}$	-3.71 ± 0.18	$\mathrm{J\,m^{-2}}$	From Calvin *et al.*	Reported InP/oleate surface formation excess. This is the surface removed when a ZnS shell replaces the original InP/ligand boundary.
$-\Gamma^\mu_{{\rm InP}/\ell}$	$+3.71 \pm 0.18$	$\mathrm{J\,m^{-2}}$	Computed sign change	Appears with a positive sign because the initial InP/ligand surface is removed. Since the original InP/ligand excess is negative, removing it raises the thermodynamic potential.
$\Delta\Gamma_0^\mu$	-7.77 ± 0.67	$\mathrm{J\,m^{-2}}$	Computed from calorimetric values	Chemical/interface part of the leading thin-shell wetting balance: $-10.07 - 1.41 + 3.71 = -7.77$. The uncertainty is propagated as $\sqrt{0.64^2 + 0.03^2 + 0.18^2} = 0.67\ \mathrm{J\,m^{-2}}$.

TABLE II. Elastic scale values used for the leading thin-shell InP/ZnS wetting-balance figure. The elastic penalty is a representative coherent-mismatch scale estimate, not a fit.

Quantity	Value used	Dimensions	Source	Explanation
f	0.08	dimensionless	Educated estimate	Representative InP/ZnS lattice-mismatch strain. Calvin *et al.* emphasize that InP/ZnS has a large lattice mismatch and that a positive strain contribution was expected. The value is used only to set the elastic scale.
h	0.807	nm	Inferred from Calvin *et al.*	Nominal shell thickness estimated as three ZnS monolayers, using 0.269 nm per monolayer.
$G_{\rm sh}$	30	GPa	Educated estimate	Representative shear modulus scale for a stiff ZnS shell. This is not fitted to calorimetry; it is used to estimate the magnitude of the coherent elastic penalty.
$K_{\rm sh}$	75	GPa	Educated estimate	Representative bulk modulus scale for a stiff ZnS shell. This is not fitted to calorimetry; it enters only through the effective thin-shell modulus.
$M_{\rm eff} = 6G_{\rm sh}/[1 + 4G_{\rm sh}/(3K_{\rm sh})]$	117.39	GPa	Computed	Effective modulus in the thin-shell coherent-mismatch penalty. With $G_{\rm sh} = 30$ GPa and $K_{\rm sh} = 75$ GPa, $M_{\rm eff} = 117.39$ GPa.
$M_{\rm eff} f^2 h$	$+0.61$	$\mathrm{J\,m^{-2}}$	Computed elastic scale	Representative coherent elastic mismatch penalty: $117.39 \times 10^9 (0.08)^2 (0.807 \times 10^{-9}) = 0.606\ \mathrm{J\,m^{-2}}$. No formal uncertainty is assigned because this is a scale estimate, not a measured quantity.
$\Delta\omega_{\rm wet} = \Delta\Gamma_0^\mu + M_{\rm eff} f^2 h$	-7.16 ± 0.67	$\mathrm{J\,m^{-2}}$	Computed net balance	Net leading-order wetting balance: $-7.77 + 0.61 = -7.16\ \mathrm{J\,m^{-2}}$. The quoted uncertainty reflects only the propagated calorimetric uncertainty in $\Delta\Gamma_0^\mu$ and does not include uncertainty in the elastic scale estimate.

TABLE III. Model values used in the finite-size calorimetry figure. Digitized Calvin *et al.* data points are not included in this table. The plotted model is $g_{\text{ex}}(A_m) = \Gamma^{\mu}_{s0}A_m + a_{\text{eff}}A_m^2/(3V_m) + bA_m^3/(9V_m^2)$. For the illustrative curve, $a_{\text{eff}} = 0$ and b is chosen so that the regularized continuation has its minimum at $R_* = 0.8$ nm.

Quantity	Value used	Dimensions	Source and explanation
Γ^{μ}_{s0}	-3.71	J m^{-2}	Reported InP/oleate surface formation enthalpy from Calvin *et al.*; used here as an enthalpic proxy for the large-radius surface grand-potential coefficient.
V_m	3.03×10^{-5}	$\text{m}^3\ \text{mol}^{-1}$	Molar volume of InP used to convert molar surface area to equivalent spherical radius through $A_m = 3V_m/R$. Estimated from $M_{\text{InP}} \simeq 145.79\ \text{g mol}^{-1}$ and $\rho_{\text{InP}} \simeq 4.81\ \text{g cm}^{-3}$, giving $V_m \simeq 30.3\ \text{cm}^3\ \text{mol}^{-1}$.
a_{eff}	0	J m^{-1}	Illustrative simplification. Setting $a_{\text{eff}} = 0$ isolates the role of the positive radius-independent coefficient b, whose one-particle contribution is $4\pi b$.
R_*	0.8	nm	Illustrative arrest radius for the regularized continuation. It is not fitted from the Calvin *et al.* data; it is chosen to show how the negative linear trend can bend over before the molecular-cluster regime.
$A_* = 3V_m/R_*$	1.14×10^5	$\text{m}^2\ \text{mol}^{-1}$	Molar surface area corresponding to the chosen arrest radius. In the plotted units this is $A_* = 113.6 \times 10^3\ \text{m}^2\ \text{mol}^{-1}$.
$b = \lvert\Gamma^{\mu}_{s0}\rvert R_*^2/3$	7.91×10^{-19}	J	Positive nonarea coefficient inside the overall 4π normalization of Eq. (147); this value places the minimum at $R_* = 0.8$ nm in the $a_{\text{eff}} = 0$ model.
b	4.94	eV	The same normalized coefficient converted using 1 eV $= 1.602176634 \times 10^{-19}$ J.
$4\pi b$	62.1	eV	Actual radius-independent contribution to the excess grand potential of one closed nanocrystal.
Plot range in A_m	20–140	$10^3\ \text{m}^2\ \text{mol}^{-1}$	Chosen to show the measured InP window and the finite-size continuation toward smaller equivalent radii.

[1] M. E. Gurtin and A. I. Murdoch, A continuum theory of elastic material surfaces, Arch. Ration. Mech. Anal. **57**, 291 (1975).

[2] M. E. Gurtin and A. I. Murdoch, Surface stress in solids, Int. J. Solids Struct. **14**, 431 (1978).

[3] M. E. Gurtin, J. Weissmüller, and F. Larché, A general theory of curved deformable interfaces in solids at equilibrium, Philos. Mag. A **78**, 1093 (1998).

[4] R. C. Cammarata and K. Sieradzki, Surface and interface stresses, Annu. Rev. Mater. Sci. **24**, 215 (1994).

[5] P. Sharma, S. Ganti, and N. Bhate, Effect of surfaces on the size-dependent elastic state of nano-inhomogeneities, Appl. Phys. Lett. **82**, 535 (2003).

[6] R. Dingreville, J. Qu, and M. Cherkaoui, Surface free energy and its effect on the elastic behavior of nano-sized particles, wires and films, J. Mech. Phys. Solids **53**, 1827 (2005).

[7] A. Javili, A. McBride, and P. Steinmann, Thermomechanics of solids with lower-dimensional energetics: On the importance of surface, interface, and curve structures at the nanoscale. A unifying review, Appl. Mech. Rev. **65**, 010802 (2013).

[8] K. Mozaffari, S. Yang, and P. Sharma, Surface energy and nanoscale mechanics, in *Handbook of Materials Modeling* (Springer Nature, Cham, Switzerland, 2019).

[9] F. D. Fischer, T. Waitz, D. Vollath, and N. K. Simha, On the role of surface energy and surface stress in phase-transforming nanoparticles, Prog. Mater. Sci. **53**, 481 (2008).

[10] J. Weissmüller, Adsorption–strain coupling at solid surfaces, Curr. Opin. Chem. Eng. **24**, 45 (2019).

[11] P. Müller and A. Saúl, Elastic effects on surface physics, Surf. Sci. Rep. **54**, 157 (2004).

[12] J. W. Gibbs, On the equilibrium of heterogeneous substances, Trans. Conn. Acad. Arts Sci. **3**, 108 (1876) and 343 (1878).

[13] A. I. Rusanov, A. K. Shchekin, and D. V. Tatyanenko, Grand potential in thermodynamics of solid bodies and surfaces, J. Chem. Phys. **131**, 161104 (2009).

[14] T. Frolov and Y. Mishin, Thermodynamics of coherent interfaces under mechanical stresses. I. Theory, Phys. Rev. B **85**, 224106 (2012).

[15] A. Navrotsky, Thermochemistry of nanomaterials, Rev. Mineral. Geochem. **44**, 73 (2001).

[16] A. Navrotsky, Energetics of nanoparticle oxides: Interplay between surface energy and polymorphism, Geochem. Trans. **4**, 34 (2003).

[17] A. Navrotsky, Nanoscale effects on thermodynamics and phase equilibria in oxide systems, ChemPhysChem **12**, 2207 (2011).

[18] D. Vollath, F. D. Fischer, and D. Holec, Surface energy of nanoparticles—Influence of particle size and structure, Beilstein J. Nanotechnol. **9**, 2265 (2018).

[19] L. Manna, L.-W. Wang, R. Cingolani, and A. P. Alivisatos, First-principles modeling of unpassivated and surfactant-passivated bulk facets of wurtzite CdSe: A model system for studying the anisotropic growth of CdSe nanocrystals, J. Phys. Chem. B **109**, 6183 (2005).

[20] C. R. Bealing, W. J. Baumgardner, J. J. Choi, T. Hanrath, and R. G. Hennig, Predicting nanocrystal shape through consideration of surface-ligand interactions, ACS Nano **6**, 2118 (2012).

[21] G. D. Barmparis, Z. Lodziana, N. Lopez, and I. N. Remediakis, Nanoparticle shapes by using Wulff constructions and first-principles calculations, Beilstein J. Nanotechnol. **6**, 361 (2015).

[22] J. J. Calvin, A. S. Brewer, M. F. Crook, T. M. Kaufman, and A. P. Alivisatos, Observation of negative surface and interface energies of quantum dots, Proc. Natl. Acad. Sci. USA **121**, e2307633121 (2024).
[23] N. C. Anderson, M. P. Hendricks, J. J. Choi, and J. S. Owen, Ligand exchange and the stoichiometry of metal chalcogenide nanocrystals: Spectroscopic observation of facile metal-carboxylate displacement and binding, J. Am. Chem. Soc. **135**, 18536 (2013).
[24] N. Kirkwood, J. O. V. Monchen, R. W. Crisp, G. Grimaldi, H. A. C. Bergstein, I. du Fossé, W. van der Stam, I. Infante, and A. J. Houtepen, Finding and fixing traps in II–VI and III–V colloidal quantum dots: The importance of Z-type ligand passivation, J. Am. Chem. Soc. **140**, 15712 (2018).
[25] J. J. Calvin, T. M. Kaufman, A. B. Sedlak, M. F. Crook, and A. P. Alivisatos, Observation of ordered organic capping ligands on semiconducting quantum dots via powder X-ray diffraction, Nat. Commun. **12**, 2663 (2021).
[26] D. Zherebetskyy, M. Scheele, Y. Zhang, N. Bronstein, C. Thompson, D. Britt, M. Salmeron, A. P. Alivisatos, and L.-W. Wang, Hydroxylation of the surface of PbS nanocrystals passivated with oleic acid, Science **344**, 1380 (2014).
[27] A. Mathur, P. Sharma, and R. C. Cammarata, Negative surface energy—Clearing up confusion, Nat. Mater. **4**, 186 (2005).
[28] Z. Łodziana, N.-Y. Topsøe, and J. K. Nørskov, A negative surface energy for alumina, Nat. Mater. **3**, 289 (2004).
[29] Z. Lin, B. Gilbert, Q. Liu, G. Ren, and F. Huang, A thermodynamically stable nanophase material, J. Am. Chem. Soc. **128**, 6126 (2006).
[30] A. Nelson and L. H. Friedman, Thermodynamically stable colloidal solids: Interfacial thermodynamics from the particle size distribution, J. Phys. Chem. C **126**, 2161 (2022).
[31] J. Weissmüller, Alloy effects in nanostructures, Nanostruct. Mater. **3**, 261 (1993).
[32] R. Kirchheim, Grain coarsening inhibited by solute segregation, Acta Mater. **50**, 413 (2002).
[33] C. E. Krill, H. Ehrhardt, and R. Birringer, Thermodynamic stabilization of nanocrystallinity, Z. Metallkd. **96**, 1134 (2005).
[34] J. R. Trelewicz and C. A. Schuh, Grain boundary segregation and thermodynamically stable binary nanocrystalline alloys, Phys. Rev. B **79**, 094112 (2009).
[35] T. Chookajorn, H. A. Murdoch, and C. A. Schuh, Design of stable nanocrystalline alloys, Science **337**, 951 (2012).
[36] T. Chookajorn and C. A. Schuh, Thermodynamics of stable nanocrystalline alloys: A Monte Carlo analysis, Phys. Rev. B **89**, 064102 (2014).
[37] C. A. Schuh and K. Lu, Stability of nanocrystalline metals: The role of grain-boundary chemistry and structure, MRS Bull. **46**, 225 (2021).
[38] R. Shuttleworth, The surface tension of solids, Proc. Phys. Soc. A **63**, 444 (1950).
[39] H. Ibach, The role of surface stress in reconstruction, epitaxial growth and stabilization of mesoscopic structures, Surf. Sci. Rep. **29**, 195 (1997).
[40] W. Haiss, Surface stress of clean and adsorbate-covered solids, Rep. Prog. Phys. **64**, 591 (2001).
[41] D. Kramer and J. Weissmüller, A note on surface stress and surface tension and their interrelation via Shuttleworth's equation and the Lippmann equation, Surf. Sci. **601**, 3042 (2007).
[42] C.-Y. Hui and A. Jagota, Surface tension, surface energy, and chemical potential due to their difference, Langmuir **29**, 11310 (2013).
[43] F. Amiot, Bridging scales between solid mechanics and surface chemistry, Sci. Rep. **12**, 10665 (2022).
[44] F. C. Larché and J. W. Cahn, A linear theory of thermochemical equilibrium of solids under stress, Acta Metall. **21**, 1051 (1973).
[45] F. C. Larché and J. W. Cahn, A nonlinear theory of thermochemical equilibrium of solids under stress, Acta Metall. **26**, 53 (1978).
[46] F. C. Larché and J. W. Cahn, The interactions of composition and stress in crystalline solids, Acta Metall. **33**, 331 (1985).
[47] Y. Mishin, Calculation of open and closed system elastic coefficients for multicomponent solids, Phys. Rev. B **91**, 224107 (2015).
[48] D. J. Steigmann and R. W. Ogden, Plane deformations of elastic solids with intrinsic boundary elasticity, Proc. R. Soc. A **453**, 853 (1997).
[49] D. J. Steigmann and R. W. Ogden, Elastic surface-substrate interactions, Proc. R. Soc. A **455**, 437 (1999).
[50] P. Chhapadia, P. Mohammadi, and P. Sharma, Curvature-dependent surface energy and implications for nanostructures, J. Mech. Phys. Solids **59**, 2103 (2011).
[51] P. M. Diehm, P. Ágoston, and K. Albe, Size-dependent lattice expansion in nanoparticles: Reality or anomaly? ChemPhysChem **13**, 2443 (2012).
[52] S.-W. Chan and W. Wang, Surface stress of nano-crystals, Mater. Chem. Phys. **273**, 125091 (2021).
[53] F. Bertolotti, D. N. Dirin, M. Ibáñez, F. Krumeich, R. Frison, O. Voznyy, E. H. Sargent, M. V. Kovalenko, A. Guagliardi, and N. Masciocchi, Crystal symmetry breaking and vacancies in colloidal lead chalcogenide quantum dots, Nat. Mater. **15**, 987 (2016).
[54] Q. Zhao, A. Hazarika, L. T. Schelhas, J. Liu, E. A. Gaulding, G. Li, M. Zhang, M. F. Toney, P. C. Sercel, and J. M. Luther, Size-dependent lattice structure and confinement properties in $CsPbI_3$ perovskite nanocrystals: Negative surface energy for stabilization, ACS Energy Lett. **5**, 238 (2020).
[55] P. B. Canham, The minimum energy of bending as a possible explanation of the biconcave shape of the human red blood cell, J. Theor. Biol. **26**, 61 (1970).
[56] W. Helfrich, Elastic properties of lipid bilayers: Theory and possible experiments, Z. Naturforsch. C **28**, 693 (1973).
[57] J. R. Rice, Thermodynamics of the quasi-static growth of Griffith cracks, J. Mech. Phys. Solids **26**, 61 (1978).
[58] J. P. Hirth and J. R. Rice, On the thermodynamics of adsorption at interfaces as it influences decohesion, Metall. Trans. A **11**, 1501 (1980).
[59] I. Langmuir, The adsorption of gases on plane surfaces of glass, mica and platinum, J. Am. Chem. Soc. **40**, 1361 (1918).
[60] T. J. Willmore, Note on embedded surfaces, Analele Ştiinţifice ale Universităţii "Al. I. Cuza" Iaşi, Secţiunea I a Matematică (N.S.) **11B**, 493 (1965).
[61] M. P. do Carmo, *Differential Geometry of Curves and Surfaces* (Prentice-Hall, Englewood Cliffs, NJ, 1976).
[62] J. Weissmüller and J. W. Cahn, Mean stresses in microstructures due to interface stresses: A generalization of a capillary equation for solids, Acta Mater. **45**, 1899 (1997).

[63] P. Reiss, M. Protière, and L. Li, Core/shell semiconductor nanocrystals, Small **5**, 154 (2009).

[64] Y.-H. Won, O. Cho, T. Kim, D. Y. Chung, T. Kim, H. Chung, H. Jang, J. Lee, D. Kim, and E. Jang, Highly efficient and stable InP/ZnSe/ZnS quantum dot light-emitting diodes, Nature (London) **575**, 634 (2019).

[65] M. Rafipoor, D. Dupont, H. Tornatzky, M. Tessier, J. Maultzsch, Z. Hens, and H. Lange, Strain engineering in InP/(Zn,Cd)Se core/shell quantum dots, Chem. Mater. **30**, 4393 (2018).

[66] M. Rafipoor, H. Tornatzky, D. Dupont, J. Maultzsch, M. Tessier, Z. Hens, and H. Lange, Strain in InP/ZnSe,S core/shell quantum dots from lattice mismatch and shell thickness: Material stiffness influence, J. Chem. Phys. **151**, 154704 (2019).

[67] H. Lange and D. F. Kelley, Spectroscopic effects of lattice strain in InP/ZnSe and InP/ZnS nanocrystals, J. Phys. Chem. C **124**, 22839 (2020).

[68] B. M. Cossairt and J. S. Owen, CdSe clusters: At the interface of small molecules and quantum dots, Chem. Mater. **23**, 3114 (2011).

[69] A. S. Mule, S. Mazzotti, A. A. Rossinelli, M. Aellen, P. T. Prins, J. C. van der Bok, S. F. Solari, Y. M. Glauser, P. V. Kumar, A. Riedinger, *et al.*, Unraveling the growth mechanism of magic-sized semiconductor nanocrystals, J. Am. Chem. Soc. **143**, 2037 (2021).